Available online at www.sciencedirect.com

SciVerse ScienceDirect

Geochimica et Cosmochimica Acta 75 (2011) 7146–7179

Geochimica et Cosmochimica Acta

www.elsevier.com/locate/gca

Re-assessing the surface cycling of molybdenum and rhenium

Christian A. Miller [a,b,*], Bernhard Peucker-Ehrenbrink [a], Brett D. Walker [a,c], Franco Marcantonio [d]

[a] Dept. of Marine Chemistry and Geochemistry, Woods Hole Oceanographic Institution, 360 Woods Hole Road, Woods Hole, MA 02543, USA
[b] Dept. of Earth, Atmospheric and Planetary Sciences, Massachusetts Institute of Technology, 77 Massachusetts Avenue, Cambridge, MA 02139, USA
[c] Dept. of Ocean Sciences, University of California Santa Cruz, Room A-312, Earth & Marine Sciences Building, Santa Cruz, CA 95064, USA
[d] Dept. of Geology and Geophysics, Texas A&M University, MS 3115, Texas A&M University, College Station, TX 77843, USA

Received 21 July 2010; accepted in revised form 13 June 2011; available online 9 September 2011

Abstract

We re-evaluate the cycling of molybdenum (Mo) and rhenium (Re) in the near-surface environment. World river average Mo and Re concentrations, initially based on a handful of rivers, are calculated using 38 rivers representing five continents, and 11 of 19 large-scale drainage regions. Our new river concentration estimates are 8.0 nmol kg^{-1} (Mo), and 16.5 pmol kg^{-1} (Re, natural + anthropogenic). The linear relationship of dissolved Re and SO_4^{2-} in global rivers ($R^2 = 0.76$) indicates labile continental Re is predominantly hosted within sulfide minerals and reduced sediments; it also provides a means of correcting for the anthropogenic contribution of Re to world rivers using independent estimates of anthropogenic sulfate. Approximately 30% of Re in global rivers is anthropogenic, yielding a pre-anthropogenic world river average of 11.2 pmol Re kg^{-1}. The potential for anthropogenic contribution is also seen in the non-negligible Re concentrations in precipitation (0.03–5.9 pmol kg^{-1}), and the nmol kg^{-1} level Re concentrations of mine waters. The linear Mo–SO_4^{2-} relationship ($R^2 = 0.69$) indicates that the predominant source of Mo to rivers is the weathering of pyrite. An anthropogenic Mo correction was not done as anthropogenically-influenced samples do not display the unambiguous metal enrichment observed for Re. Metal concentrations in high temperature hydrothermal fluids from the Manus Basin indicate that calculated end-member fluids (i.e. Mg-free) yield negative Mo and Re concentrations, showing that Mo and Re can be removed more quickly than Mg during recharge. High temperature hydrothermal fluids are unimportant sinks relative to their river sources 0.4% (Mo), and 0.1% (pre-anthropogenic Re). We calculate new seawater response times of 4.4×10^5 yr (τ_{Mo}) and 1.3×10^5 yr (τ_{Re}, pre-anthropogenic).

1. INTRODUCTION

The association between organic carbon (C_{org}) and "redox-sensitive" metals such as V, Cr, Zn, Mo, Cd, Re, and U is widely documented in both modern and ancient sediments, where these metals are used to infer the redox characteristics of the depositional and diagenetic environments (Bertine and Turekian, 1973; Klinkhammer and Palmer, 1991; Calvert and Pederson, 1993; Colodner et al., 1993a; Crusius et al., 1996; Quinby-Hunt and Wilde, 1996; Morford and Emerson, 1999; Jaffe et al., 2002; Tribovillard et al., 2006; Morford et al., 2007). Because the burial and weathering of sedimentary C_{org} is a significant sink and source of atmospheric CO_2 on geological timescales (Rubey, 1951; Walker et al., 1981; Berner and Raiswell, 1983), redox-sensitive metals offer another way of evaluating C_{org} cycling throughout geologic time. Molybdenum and Re are particularly valuable as they show minimal detrital influence, exhibit the greatest enrichment in reducing sediments, are conservative in seawater, and

* Corresponding author. Address: Dept. of Terrestrial Magnetism, Carnegie Institution of Washington, 5241 Broad Branch Road NW, Washington, DC 20015, USA.
E-mail address: xian.miller75@gmail.com (C.A. Miller).

0016-7037/$ - see front matter © 2011 Elsevier Ltd. All rights reserved.
doi:10.1016/j.gca.2011.09.005

have seawater response times sufficiently long to yield globally-integrated information (Morris, 1975; Collier, 1985; Anbar et al., 1992; Colodner et al., 1993a; Jones and Manning, 1994; Crusius et al., 1996; Morford and Emerson, 1999; Tribovillard et al., 2006).

The application of redox-sensitive metals to modern and paleoenvironments has become increasingly specific and quantitative. For example, Algeo and Lyons (2006) use the relationship between Mo and C_{org} to quantify the concentration of H_2S in bottom waters; analyses of stable isotope variations of Mo have been used to develop a paleoredox proxy (Siebert et al., 2003; Arnold et al., 2004; Nägler et al., 2005; Poulson et al., 2006; Neubert et al., 2008; Pearce et al., 2008), while isotopes of Re have been shown to vary systematically across a redox gradient (Miller, 2009). The increasingly informative application of Mo and Re to paleoenvironmental problems is contingent on understanding their present-day cycling in near-surface reservoirs. This study re-evaluates the surface cycling of Re and Mo, with particular attention to their riverine source to seawater and resulting seawater response times.

2. BACKGROUND: SURFACE CYCLING OF MOLYBDENUM AND RHENIUM

Both Mo and Re are present in modern seawater as the oxyanions molybdate and perrhenate (MoO_4^{2-} and ReO_4^-, respectively; Łetowski et al., 1966; Brookins, 1986). Despite the incorporation of Mo into nitrogenase (Kim and Rees, 1992; Einsle et al., 2002) and the bio-accumulation of Re in certain seaweeds (Fukai and Meinke, 1962; Yang, 1991) neither element is a major nutrient and both are conservative in seawater (Morris, 1975; Collier, 1985; Anbar et al., 1992; Colodner et al., 1993a; Tuit, 2003). The seawater concentrations of Mo and Re are 104 nmol kg^{-1} and 40 pmol kg^{-1}, respectively (Morris, 1975; Collier, 1985; Koide et al., 1987; Anbar et al., 1992; Colodner et al., 1993a, 1995).

The seawater response time (*aka* residence time) of an element is the ratio of its seawater inventory and its flux to or from seawater (Rodhe, 1992). Fluxes of Mo and Re from seawater are very poorly constrained (Morford and Emerson, 1999), so response times have been determined using riverine fluxes to seawater. The world river average Mo concentration was estimated at 4.5 nmol kg^{-1} (Bertine and Turekian, 1973), while that of Re was estimated at 2.1 pmol kg^{-1} (original estimate by Colodner et al., 1993a was 2.3 pmol kg^{-1}; this was then revised down by 10% due to a miscalibration of the ^{185}Re spike as described in Colodner et al., 1995). Using an oceanic volume of 1.332×10^{21} L (Charette and Smith, 2010) and a global river water flux of 3.86×10^{16} L yr^{-1} (Fekete et al., 2002), these estimates correspond to Mo and Re seawater response times of 8.7×10^5 yr and 7.2×10^5 yr. These are similar to the reported Mo and Re response times of 8.0×10^5 yr and 7.5×10^5 yr (Colodner et al., 1993a; Morford and Emerson, 1999).

Using hydrothermal water flux values from Elderfield and Schultz (1996) and Mo concentrations from Metz and Trefry (2000), Wheat et al. (2002) estimate respective high- and low-temperature hydrothermal Mo fluxes of about 1% and 13% the Mo riverine flux. Incorporation of this 14% flux increase decreases the response time of Mo in seawater to $\sim 7.6 \times 10^5$ yr. Prior to this study, there were no equivalent data for Re, though Ravizza et al. (1996) considered hydrothermal fluxes to be unimportant.

Though they are crucial components of mass balance and modeling studies (e.g. Morford and Emerson, 1999; Algeo and Lyons, 2006), global Mo and Re river fluxes are poorly constrained. The world river Mo average is based on three rivers (Amazon, Congo, and Maipo; Bertine and Turekian, 1973), while that of Re is based on four (Amazon, Orinoco, Brahmaputra, and Ganges; Colodner et al., 1993a). Previous river concentration estimates, therefore, sampled only ~23% of the global runoff and are heavily biased by the Amazon. Though subsequent studies of Re have shown much higher riverine concentrations and a large concentration range (Colodner et al., 1995; Dalai et al., 2002; Rahaman and Singh, 2010), a thorough re-evaluation of world river average Mo and Re concentrations has not been done; that is the principal aim of this study.

3. MATERIALS AND METHODS

3.1. Sample collection

River samples were collected according to opportunity (locations in Fig.1). Large exorheic rivers were sampled with the goal of obtaining a significant proportion of the global riverine flux, while smaller rivers were used to estimate the range of Mo and Re concentrations. Time-series samples of Arctic rivers and major tributaries of the Mississippi were collected by the Student Partners Project and Grzymko et al. (2007). Precipitation (rain and snow) samples were collected on Cape Cod, USA; "mine waters" were collected from the Berkeley Pit, Montana, USA, and from the Kupferschiefer deposit, Mansfeld, Germany; high temperature seafloor hydrothermal fluid samples were taken at the Papua New Guinea–Australia–Canada–Manus (PACMANUS) hydrothermal field.

Samples were taken under metal free conditions using a high-density polyethylene bottle (HDPE) for sampling, sterile plastic syringes (HSW, NORM-JECT®) and sterile plastic filter cartridges (Millipore® Sterivex™, 0.22 or 0.45 μm) for filtration, and certified clean 125 mL HDPE bottles (EP Scientific Products) for storage. With the exception of the collection vessel, all materials were single-use and were pre-treated with sample material before being used to process the collected sample aliquot. In general, samples were not acidified, and were kept refrigerated at about 4 °C.

3.2. Mo and Re concentrations

Concentrations of Mo and Re were determined by isotope dilution (ID) inductively-coupled plasma mass spectrometry (ICP-MS). Approximately 20 g of sample material was weighed into a clean bottle, spiked with ^{95}Mo and ^{185}Re spikes in 5% HNO_3, and equilibrated for 2 days in an oven at 60 °C.

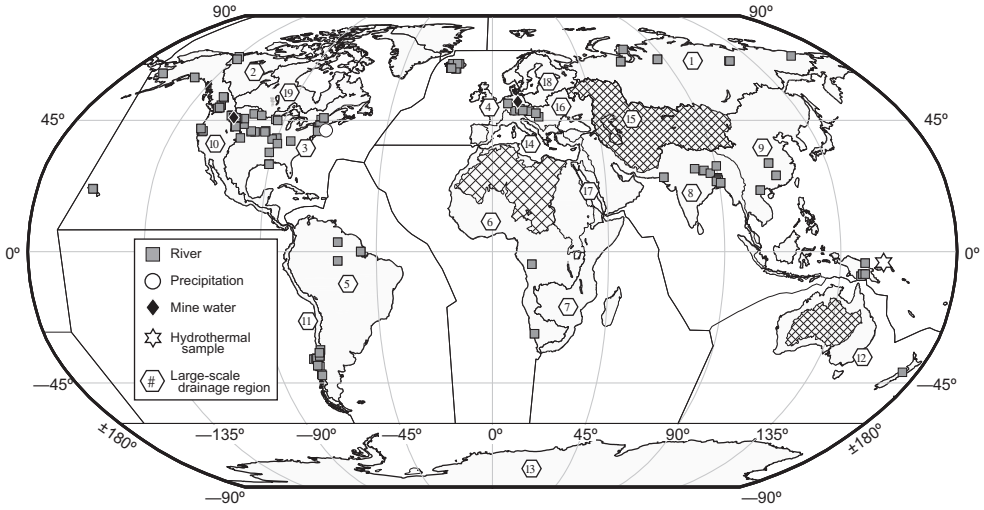

Fig. 1. Locations for river, precipitation, mine water, and hydrothermal fluid samples analyzed for this study. Internally-draining continental areas (i.e. non-exorheic) are hatched-out. Also shown are borders for the large-scale drainage regions (after Graham et al., 1999; data from http://www.ngdc.noaa.gov/ecosys/cdroms/graham/graham/graham.htm#element7).

Chromatographic purification used 1 mL (wet volume) of pre-cleaned Biorad AG 1 × 8, 100–200 mesh anion resin (after Morgan et al., 1991). Chromatography was optimized for quantitative recovery of Re as Mo is typically three orders of magnitude more abundant in natural waters (Kharkar et al., 1968; Bertine and Turekian, 1973; Morris, 1975; Collier, 1985; Anbar et al., 1992; Colodner et al., 1993a). Recovery of Mo, though not quantitative, was sufficient to obtain Mo ion beams larger than those of Re. All Mo and Re analyses were done with the ELEMENT 2 mass spectrometer (Thermo Fisher Scientific) in the ICP-MS facility. Samples were introduced using a perfluoroalkoxy (PFA) MicroFlow nebulizer (Elemental Scientific Incorporated), a quartz spray chamber, and regular cones (Ni). Masses 95 (Mo), 97 (Mo), 98 (Mo), 185 (Re), 187 (Re), 188 (Os), and 101 (Ru) were scanned 100 times in low mass resolution; each nuclide was counted for a total of 2 s. Mass 188 count rates were uniformly low, so no correction is made for ^{187}Os. Acid blanks and standards were analyzed every five or six samples to correct for blank contributions as well as instrumental mass fractionation using natural Mo and Re isotopic ratios (Rosman and Taylor, 1998).

Uncertainties of Mo and Re concentration measurements were estimated using multiple ($n = 12$) analyses of processed aliquots of a St. Lawrence sample from Côteau du Lac, Québec, Canada; Mo and Re uncertainties are 6.2% and 4.6% (2 SD), respectively. This is similar to the Re concentration uncertainty of 4% reported by Colodner et al. (1993b).

3.3. Cation concentrations

Where feasible, concentrations of major (Na^+, Mg^{2+}, K^+, Ca^{2+}) and selected minor and trace cations (Rb^+, Sr^{2+}, and Ba^{2+}) were determined by ID ICP-MS. Isotope dilution determination of Na was not possible as it is mono-isotopic; ID determination of K was complicated by significant up-mass tailing of ^{40}Ar on to ^{41}K; ID determination of both Rb and Sr would have doubled the number of analyses due to the isobars at mass 87. Concentrations of Na, K, and Rb were determined by standard-calibration ICP-MS using ^{23}Na, ^{39}K, and ^{85}Rb.

Sample aliquots of 1 mL were spiked with mixed ^{25}Mg–^{135}Ba and ^{42}Ca–^{84}Sr, diluted 10-fold with 5% HNO_3, and heated at 60 °C for 2 days to ensure spike-sample equilibration. No purification chemistry was done.

Cation analyses were performed with the ELEMENT 2 ICP-MS (Thermo Fisher Scientific) in the WHOI ICP-MS facility. Samples were introduced using a PFA MicroFlow nebulizer (Elemental Scientific Incorporated), a quartz spray chamber, and regular cones (Ni). Data were taken in low, medium, and high mass resolution. Low resolution evaluated masses 23 (Na), 24 (Mg), 25 (Mg), 26 (Mg), 82 (Kr), 83 (Kr), 84 (Kr + Sr), 85 (Rb), 86 (Kr + Sr), 87 (Rb + Sr), 88 (Sr), 135 (Ba), 137 (Ba), and 138 (Ba); as with Mo and Re, ion beam intensities are measured across 20 channels of the central 5% of the peak. Medium resolution evaluated masses 42 (Ca), 43 (Ca), 44 (Ca), and 48 (Ca) by integrating the ion beam intensity of the entire peak. High resolution evaluated masses 23 (Na), 24 (Mg), 25 (Mg), 26 (Mg), and 39 (K) as whole peak integrations.

At the beginning of an analytical sequence, five-point standard calibration curves of ^{23}Na, ^{39}K, and ^{85}Rb were constructed to evaluate these elements. Nuclide transmission in the ELEMENT 2 is a function of mass and closely follows a power law. Calibration curves were highly linear ($R^2 > 0.99$) across the counting-analog mode transition of the secondary electron multiplier. The duration of a typical analytical sequence (43 samples, 5 standards, 49 rinse acid blanks) was ~12 h. Standards evaluated during and after a sequence indicated no significant instrumental drift.

As an internal consistency check, spike-unmixing of Mg, Ca, Sr, and Ba is done with multiple isotope ratios. ^{23}Sodium was measured in both low and high resolution for the same reason; unfortunately this was not done for K

as proximity to the ^{40}Ar peak restricts ^{39}K acquisition to high resolution, or for Rb as even low-resolution ^{85}Rb signal intensities seldom exceeded 10 times the intensity in the rinse acid blanks, preventing the acquisition of good data in medium resolution.

Uncertainties were estimated using multiple sample aliquot processing ($n = 22$) and analyses ($n = 33$) of a St. Lawrence sample from Côteau du Lac, Québec, Canada. Uncertainties of Na, Mg, Ca, K, Rb, Sr, and Ba are 14%, 1.3%, 10%, 16%, 15%, 20%, and 7% (2 SD) respectively. The uncertainty for Sr concentration is very large considering analyses are done by ID; this is due to the ~60% contribution of ^{84}Kr to the mass 84 ion beam intensity.

3.4. Anion concentrations

Concentrations of Cl^- and SO_4^{2-} were determined by standard-calibration using a Dionex® DX-500 ion chromatography system comprised of an ED 40 Electrochemical Detector, a GP 50 Gradient Pump, an LC 30 Chromatography oven, an IonPac® AS15 4-mm chromatographic column and an ASRS®-ULTRA II 4-mm suppressor. All analyses were done in the laboratory of Dr. J. Seewald, WHOI.

Five milliliters of sample fluid were loaded into a clean plastic Dionex® vial, allowing three separate sample injections per vial. Samples were eluted with a 60:40 (v/v) mixture of 50 mmol L^{-1} NaOH and H_2O (Milli-Q®). Standards were analyzed after every nine sample injections (~2 h), and were used to construct three-point calibration curves. Sample concentrations that exceeded the calibration range are diluted and reanalyzed. Reproducibilities of Cl^- and SO_4^{2-} for the most dilute standard are 3.4% and 4.3% respectively (2 SD, $n = 74$); reproducibilities for a St. Lawrence River sample ($n = 69$) are similar to those of the most similar (most concentrated) calibrating standard.

Table 1A
Basin characteristics and sampling locations for exorheic rivers evaluated in this study. Rivers are listed by large-scale drainage region as described by Graham et al. (1999), and then alphabetically. Data for riverine water fluxes (fH_2O) and suspended sediment fluxes (fSediment) are from Meybeck and Ragu (1995) and Peucker-Ehrenbrink (2009).

River	Large-scale drainage region	Continent	fH_2O ($km^3\ yr^{-1}$)	Drainage area (km^2)	fSediment ($Pg\ yr^{-1}$)	Latitude (decimal °)	Longitude (decimal °)
Kolyma	1	Asia	132	653,500	10.1	66.5414	002.6458
Lena	1	Asia	530	2,441,816	20.7	66.7664	123.3967
Ob	1	Asia	404	2,760,465	15.5	66.5414	066.4722
Yenisei	1	Asia	620	2,579,365	4.7	67.4344	086.3908
Mackenzie	2	North America	307	1,712,738	124	67.4521	−133.7389
Connecticut	3	North America	14.2	26509.5	–	41.4853	−072.5142
Housatonic	3	North America	2.4	2500	0.5	41.3852	−072.5066
Hudson	3	North America	17.3	34,000	0.6	42.7611	−073.9700
Mississippi	3	North America	529	3,270,000	450	29.9208	−090.1353
Saint Lawrence	3	North America	447	1,100,000	3.8	45.8586	−073.2397
Ölfusà	4	Europe	13.9	6000	–	63.9383	−021.0083
Rhine	4	Europe	69.4	185,000	2.8	50.9481	006.9714
Þjórsà	4	Europe	12.6	6981.5	–	63.9300	−020.6400
Amazon	5	South America	6590	6133120.0	1175.0	00.0333	−051.0500
Orange	6	Africa	11.4	945,000	89	−28.0833	016.8917
Zaire/Congo	6	Africa	1200	3,710,000	32.8	−04.2990	015.2777
Brahmaputra	8	Asia	510	595,000	630	24.4084	089.7986
Ganga	8	Asia	493	1,033,052	522	24.0553	089.0314
Indus	8	Asia	57	1025866.5	250	25.4422	068.3164
Meghna	8	Asia	111.0	87500.0	–	23.5993	090.6102
Fly	9	Oceania	141	64,500	110.0	−08.4150	143.2422
Kikori	9	Oceania	40	13,200	–	−07.6809	144.8352
Pearl	9	Asia	7.8	17,200	0.8	26.1153	113.2681
Purari	9	Oceania	84.13	31,000	90	−07.7017	143.8317
Red	9	Asia	123	162,500	123	21.0544	105.8472
Sepik	9	Oceania	120	78,350	44.08	−03.9051	144.5403
Yangtze	9	Asia	928	1,808,000	490	30.2872	111.5264
Copper	10	North America	34.1	62,678	70	60.4453	−145.0667
Fraser	10	North America	112	236,350	17.2	49.5056	−121.4142
Yukon	10	North America	205	847,642	60	61.9486	−162.9077
Andalien	11	South America	0.48	~850	–	−36.8019	−073.9667
Biobío	11	South America	31.69	24,782	–	−36.8088	−073.0979
Itata	11	South America	11.39	11,385	–	−36.6242	−072.6957
Maipo	11	South America	3.14	15,157	–	−33.6288	−070.3548
Maule	11	South America	17.96	20,865	–	−35.7236	−071.1763
Tinguiririca (trib. of Rapel)	11	South America	5.38	15,157	–	−34.6125	−070.9818
Tolten	11	South America	18.4	8040	–	−39.0109	−073.0818
Danube	16	Europe	207	802,843	68	47.5000	019.0500

Table 1B
List of exorheic rivers and chemical data used to re-evaluate Mo and Re world river averages. Chemical data are listed to the last significant digit. Where the last significant digit is zero, this is indicated by a decimal point or scientific notation. Uncertainties are as listed in Section 3. Entries for Rb and Sr listed as "b.d." were below the detection limits.

River	Mo (nmol kg^{-1})	Re (pmol kg^{-1})	Cl (μmol kg^{-1})	SO_4 (μmol kg^{-1})	Na (μmol kg^{-1})	Mg (μmol kg^{-1})	Ca (μmol kg^{-1})	K (μmol kg^{-1})	Rb (nmol kg^{-1})	Sr (nmol kg^{-1})	Ba (nmol kg^{-1})
Kolyma	1.47	2.9	92	100.	55	870	250	15	b.d.	230	42
Lena	3.0	2.9	260	96	370	178	380	16	5.3	800	78
Ob	3.9	12.5	135	83	3.0×10^2	185	460	28	4.7	5.0×10^2	66
Yenisei	3.5	6.5	168	73	2.0×10^2	131	360	10	1.0	600	49
Mackenzie	10.1	16.2	240	380	350	358	870	23	7	1300	280
Connecticut	7.8	14.4	–	–	–	–	–	–	–	–	–
Housatonic	5.5	6.7	–	–	–	–	–	–	–	–	–
Hudson	3.2	7.2	660	125	–	–	–	–	–	–	–
Mississippi	21	57	640	510	–	–	–	–	–	–	–
Saint Lawrence	12.1	24	580	230	520	292	810	35	10.	1200	109
Ölfusà	1.04	1.74	153	24	3.0×10^2	565	1.0×10^2	12	2.0	b.d.	3300
Rhine	10.8	57	1210	4.0×10^2	800	356	1.5×10^3	78	24	2600	190
Þjórsà	4.1	4.1	86	61	320	631	1.0×10^2	11	b.d.	b.d.	13
Amazon	0.89	1.8	–	92	10.	678	170	30.	40.	150	240
Orange	24	37	2800	1210	3700	1090	1.0×10^3	64	1.9	2.0×10^3	330
Zaire/Congo	0.45	3.0	36	18	9	621	53	39	31	17	79
Brahmaputra	11.1	4.4	43	156	180	217	620	58	27	500	89
Ganga	10.7	3.9	67	79	220	194	620	79	14	450	140
Indus	36	29	840	57	530	472	1.1×10^3	110	7	5700	3.0×10^2
Meghna	2.4	1.40	80.	50.	240	146	240	31	17	170	45
Fly	59	53	–	190	210	118	870	20.	5.6	90	70.
Kikori	3.5	9.3	–	17	5.5	281	1.1×10^3	9	5.4	90	37
Pearl	12.3	10.9	220	174	320	65.8	410	84	110	170	90
Purari	4.0	3.4	–	87	750	278	710	40	13	70	53
Red	6.7	13.3	68	126	170	218	750	44	28	1100	190
Sepik	2.0	1.64	–	–	610	243	250	24	14	18	89
Yangtze	15.8	55	310	420	440	373	700	47	15	1700	240
Copper	14.4	9.3	53	220	110	107	520	36	11	22	85
Fraser	7.9	5.3	21	98	9	126	410	16	10.	50	57
Yukon	12.0	13.4	65	280	120	297	790	38	21	60	230
Andalién	1.26	7.2	153	6.2	510	162	320	36	15	80	57
Biobío	2.3	4.9	95	47	220	100.	190	26	24	27	18
Itata	4.7	1.14	190	16.3	550	283	280	34	14	90	0 73
Maipo	33	53	2500	3300	3.0×10^2	387	3.7×10^3	70.	70	1.0×10^4	86
Maule	19	7.4	190	1740	370	129	290	33	46	44	22
Tinguiririca (trib. of Rapel)	14.4	20.	139	460	280	112	510	28	41	70	23
Toltén	4.6	1.88	41	21	170	65.7	110	22	21	16	17
Danube	10.8	74	1830	1030	2.0×10^3	1.20×10^3	1.9×10^3	160	32	3300	4.0×10^2

Table 2
Mo, Re, and Mg chemical data for four hydrothermal fluid samples from the Roman Ruins vent site, PACMANUS, Manus Basin.

Vent orifice	Mo (nmol kg^{-1})	Re (pmol kg^{-1})	Solution mass (g)	Total Mo[a] (nmol)	Total Re[a] (pmol)	Total Mo (nmol)	Total Re (pmol)	Mo[b] (nmol kg^{-1})	Re[b] (pmol kg^{-1})	Mg[c] (mmol kg^{-1})	End-member Mo[d] (nmol kg^{-1})	End-member Re[d] (pmol kg^{-1})
RMR 1 Fluid[e]	4.3	1.5	750	3.2	1.1							
RMR 1 Dregs	640	72	25.769	16	1.9							
RMR 1 Bttl Fltrt	51	23	29.1013	2.1	0.94							
Σ RMR 1						21	4	29	5.3	8.7	10.	−0.038
RMR 2 Fluid[e]	3.3	14.4	750	2.5	10.8							
RMR 2 Dregs	630	8.9	25.351	16	0.22							
RMR 2 Bttl Fltrt	82.2	97.4	29.1032	4.61	5.46							
Σ RMR 2						23	16	31	22	27	−27	5.6
RMR 3 Fluid[e]	3.7	0.65	750	2.8	0.48							
RMR 3 Dregs	180	10.8	111.933	20.	1.21							
RMR 3 Bttl Fltrt	49	12.7	28.4873	1.8	0.470							
Σ RMR 3						25	2	33	2.9	6.2	19	−0.92
RMR 4 Fluid[e]	14.9	0.82	750	11.2	0.61							
RMR 4 Dregs	1730	26	20.93	36.2	0.54							
RMR 4 Bttl Fltrt	111	12.5	28.9633	3.82	0.432							
Σ RMR 4						51	2	68	2.1	4.6	58	−0.69
Bottom H_2O	117.5	33								54.0		

[a] For fluid and dregs subcomponents, total Mo and Re inventories are calculated by multiplying the concentrations and solution masses, however because the bottle filtrate fractions were not obtained from filtering the entire 750 g of fluid, the following scaling factors are applied to the bottle filtrate solution masses (the solution mass filtered is the denominator):

RMR 1: factor = 750 g/539.16 g = 1.3911,
RMR 2: factor = 750 g/389.52 g = 1.9255,
RMR 3: factor = 750 g/578.27 g = 1.2970,
RMR 4: factor = 750 g/628.44 g = 1.1934.

[b] Calculated assuming an initial solution mass of 750 g.
[c] Mg concentration data are from Craddock et al. (2010).
[d] Calculated assuming bottom water Mg, Mo, and Re concentrations determined for the bottom water sample ("Bottom H_2O"; see above).
[e] Fluid samples were collected in August and September 2006 at approximately −3.7225°S, 151.6750°W. Temperature and pH (recalculated to 25 °C) listed below are from Craddock et al. (2010).

RMR 1: T = 314 °C, pH = 2.4,
RMR 2: T = 272 °C, pH = 2.7,
RMR 3: T = 278 °C, pH = 2.5,
RMR 4: T = 341 °C, pH = 2.6.

Table 3A
Water fluxes, water flux proportions, and average chemical concentrations for rivers of large-scale drainage region 1 (after Graham et al., 1999). The method of calculating flux-weighted regional chemical averages used in this study is also shown.

River name	fH_2O ($\times 10^{12}$ kg yr^{-1})	fH_2O[a] (proportion)	Individual river: chemical concentration averages							
			Mo (nmol kg^{-1})	Re (pmol kg^{-1})	Cl (μmol kg^{-1})	SO_4 (μmol kg^{-1})	Na (μmol kg^{-1})	Mg (μmol kg^{-1})	Ca (μmol kg^{-1})	K (μmol kg^{-1})
Kolyma	132	0.046	1.47	2.9	92	100.	55	87	250	15
Lena	530	0.185	3.0	2.9	260	96	370	178	380	16
Ob	404	0.141	3.9	12.5	135	83	3.0×10^2	185	460	28
Yenisei	620	0.217	3.5	6.5	168	73	2.0×10^2	131	360	10.
Σ_{fH_2O}	1686	0.589								
			Individual river: annual chemical fluxes (i.e. $[X]_{river} \times fH_2O_{river}$)[b]							
			nmol yr^{-1} $\times 10^{15}$	pmol yr^{-1} $\times 10^{14}$	μmol yr^{-1} $\times 10^{13}$	μmol yr^{-1} $\times 10^{13}$	μmol yr^{-1} $\times 10^{12}$	μmol yr^{-1} $\times 10^{13}$	μmol yr^{-1} $\times 10^{13}$	μmol yr^{-1} $\times 10^{12}$
Kolyma			1.94	3.8	1.2	1.33	7.2	1.2	3.3	2.0
Lena			16	15	14	5.1	2.0×10^2	9.44	20.	8.2
Ob			16	50.3	54.4	3.4	120	7.46	19	11
Yenisei			22	40.	10.4	4.5	130	8.15	23	6.4
		$\Sigma_{chemical\ fluxes}$	54.8	110.	30.7	14.3	450.	26.2	64.6	27.8
			Large-scale drainage region: chemical concentration averages (i.e. $\Sigma_{chemical\ fluxes} \div \Sigma_{fH_2O}$)[c]							
			nmol kg^{-1}	pmol kg^{-1}	μmol kg^{-1}	μmol kg^{-1}	μmol kg^{-1}	μmol kg^{-1}	μmol kg^{-1}	μmol kg^{-1}
		Region 1 averages	3.3	6.5	182	85	270	155	380	16

[a] Proportions of H_2O fluxes are the individual river fluxes divided by the regional sum (in this case, 2860.8 km^3 yr^{-1} or 2860.8×10^{12} kg yr^{-1}). Individual river fluxes are taken from the compilation of Meybeck and Ragu (1995) while the large-scale drainage region 1 flux (after Graham et al., 1999) is from Peucker-Ehrenbrink (2009).

[b] Individual river chemical fluxes are obtained by multiplying the individual river chemical concentrations by the yearly riverine H_2O fluxes.

[c] Large-scale drainage region chemical concentration averages are obtained by taking the sum of the individual fluxes for the drainage region ($\Sigma_{chemical\ fluxes}$), and dividing by the sum of the H_2O fluxes (Σ_{fH_2O}). The result is a flux-weighted chemical concentration for that portion of the large-scale drainage region that has been sampled (in this case 58.9% of the total regional H_2O flux) that is then applied to the water flux for the entire large-scale drainage region when determining global river average concentrations (see Table 3B).

Table 3B
Water fluxes, water flux proportions, and average regional chemical concentrations for all large-scale drainage regions (after Graham et al., 1999) for which data are presented in this study. Resulting world river chemical concentrations are also shown.

Graham region	fH_2O ($km^3\ yr^{-1}$)	fH_2O[a] (proportion)	Large-scale drainage region chemical concentration averages[b]							
			Mo (nmol kg^{-1})	Re (pmol kg^{-1})	Cl (μmol kg^{-1})	SO_4 (μmol kg^{-1})	Na (μmol kg^{-1})	Mg (μmol kg^{-1})	Ca (μmol kg^{-1})	K (μmol kg^{-1})
1	2855.8	0.082	3.2	6.5	182	85	270	155	380	16
2	846.1	0.024	10.1	16.2	240	380	350	358	870	23
3	2687.8	0.077	16.5	41	6.0×10^2	380	5.0×10^2	282	780	34
4	821.7	0.024	8.5	42	910	3.0×10^2	670	274	1100	60
5	10898.6	0.313	0.89	1.83	–	92	1.0×10^2	67.8	160	30
6	2426.9	0.070	0.68	3.3	63	29	120	71.8	62	40.
8	4050.7	0.116	11.3	5.1	95	134	220	213	6.0×10^2	70.
9	7001.3	0.201	17.0	42	283	330	410	314	690	41
10	1688.3	0.049	10.9	10.4	50.	220	110	224	640	31
11	1128.5	0.032	8.4	7.0	2.0×10^2	2.0×10^2	380	133	350	29
16	403.5	0.012	10.8	74	1830	1030	2.0×10^3	1200	1900	160
	Global River Average[c]		8.0	16.5	190	190	270	193	470	38

[a] Proportions of H_2O fluxes are the individual regional fluxes divided by their sum (34,809 $km^3\ yr^{-1}$). Note that though we do not have samples for regions 7, 12, 13, 14, 15, 17, 18, and 19, the sum of the H_2O fluxes for the regions sampled for this study is ~90% of the total exorheic H_2O flux.
[b] The method by which regional chemical averages are calculated is shown in detail in Table 3A.
[c] The global chemical averages are calculated in the same manner as the regional averages (see Table 3A). The regional chemical flux contributions are calculated, then summed and divided by the sum of the regional H_2O fluxes.

Table 4A
Comparison of world river average concentrations of major ions estimated using different data sets and calculated using different methods of extrapolation.

Source	Published: Meybeck (1979)	Published: Livingstone (1963)	Calculated: data from Meybeck and Ragu (1995)			Calculated: data from this study, see Table 1		
			Scaled to global H_2O flux	Scaled to area, Continents	Scaled to area, Lrg-Scl Drng Rgn[a]	Scaled to global H_2O flux	Scaled to area, Continents	Scaled to area, Lrg-Scl Drng Rgn[a]
Cl (μmol kg^{-1})	230	220	240	270	280	270	3.0×10^2	190
SO_4 (μmol kg^{-1})	120	117	117	126	137	156	2.0×10^2	190
Na (μmol kg^{-1})	310	270	280	310	330	210	330	270
Mg (μmol kg^{-1})	150	170	160	180	180	148	225	193
Ca (μmol kg^{-1})	367	370	370	420	420	350	510	470
K (μmol kg^{-1})	36	59	38	38	67	34	41	38

[a] Refers to the large-scale drainage regions described in Graham et al. (1999) and Peucker-Ehrenbrink et al. (2007).

Table 4B
Comparison of published world river average concentration estimates for minor cations as well as for the elements of interest (Mo, Re) with those calculated from this study using different methods of extrapolation; none have been corrected for anthropogenic metal contributions. Best estimates, extrapolated to large-scale drainage region, are underlined.

Source	Published: Bertine and Turekian (1973) and Colodner et al. (1993a)	Published: Gaillardet et al. (2003)	Calculated: data from this study, see Table 1		
			Scaled to global H_2O flux	Scaled to area, Continents	Scaled to area, Lrg-Scl Drng Rgn[a]
Rb (nmol kg^{-1})		19.1	28	23	24
Sr (nmol kg^{-1})		685	500	700	700
Ba (nmol kg^{-1})		170	190	180	180
Mo (nmol kg^{-1})	4.5		5.5	7.6	<u>8.0</u>
Re (pmol kg^{-1})	2.1		11.5	17.3	<u>16.5</u>

[a] Refers to the large-scale drainage regions described in Graham et al. (1999) and Peucker-Ehrenbrink et al. (2007).

4. RESULTS

Data for this study are presented in Tables 1–4 and A.5–A.8. Exorheic river data used to recalculate the world river average concentrations of Mo and Re are presented in Table 1. Chemical data for time-series samples of North American and Russian Arctic rivers, as well as for the Mississippi (Table 1) are determined by calculating flux weighted chemical averages using the time-series data presented in Table A.5. Data for Mo and Re in hydrothermal fluids (high temperature, Manus Basin) are presented in Table 2. Hydrothermal data include fluid component data as well as concentration and mass-balance information for two categories of precipitating sulfide (i.e. rapidly-precipitating "dregs" and slowly-precipitating "bottle filtrate"). Aqueous and sulfide components are all necessary to reconstitute the original sampled fluid. Also shown are the Mg data used to correct for entrained seawater (Craddock et al., 2010). Table A.6 presents data for major rivers, minor rivers, and tributaries from around the globe in an attempt to capture the global variability in Mo and Re concentration. Data for precipitation samples (Falmouth, MA, USA) and waters associated with mining (the Berkeley Pit, Butte, MT, USA and the Kupferschiefer, Mansfeld, Germany) are shown in Table A.8.

5. DISCUSSION

5.1. Complexities in determining global river characteristics

Studies estimating average river composition at the global scale assume the river subset being studied is representative of the global average. The total global river H_2O flux of 3.86×10^{16} L yr^{-1} (Fekete et al., 2002) is composed of tens of thousands of rivers and streams, so estimates are made using a smaller global river sample subset. When using small numbers of rivers, precautions should be taken to identify and minimize biases introduced by the sampling of large individual rivers taken at specific times and locations.

It has been proposed that when >50% of the global river water flux or exorheic drainage area is accounted for, direct extrapolation of flux-weighted averages to the globe is appropriate (Meybeck and Helmer, 1989). Using the data of Meybeck and Ragu (1995), this is achieved by sampling the world's largest 28 (water flux) or 296 (drainage area) rivers. If <50% of water flux or continental area is accounted for, extrapolation is done to some set of sub-regions, such as distinctive morphoclimatic areas (Meybeck, 1979), the continents (Livingstone, 1963; Berner and Berner, 1987), or sub-continental-scale drainage regions (after Graham et al., 1999). These regional values are then summed to

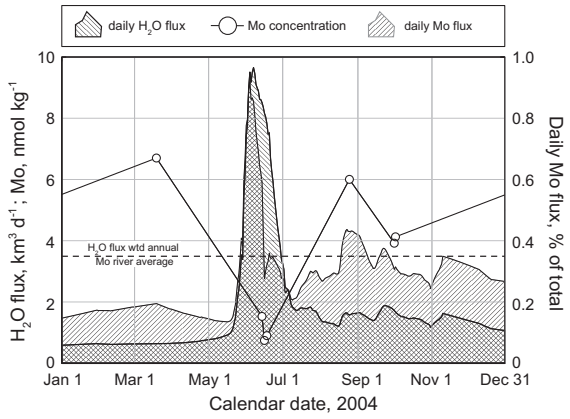

Fig. 2. Fluxes of H_2O and Mo, as well as Mo concentrations for the Yenisei River, 2004. Water flux data are from http://rims.unh.edu/ (see footnotes, Table A.5). Intervals between Mo measurements are interpolated linearly (point-to-point). Daily Mo fluxes are the product of daily H_2O fluxes and interpolated or measured Mo concentrations. These daily fluxes are summed and divided by the yearly H_2O flux to determine flux-weighted yearly average Mo concentration (dashed line).

account for global runoff. If possible, rivers should be sampled in an attempt to capture the large *inter*-river variability caused by differences in basin morphology, climate, and geology.

There is also significant *intra*-river variability; one sampling event represents a single snapshot of the river in time and space, and a temporal–spatial integration of the river should therefore be attempted where possible. Obtaining spatially integrated samples is theoretically simple; samples obtained at the river mouth are representative of the entire drainage region. Truly reliable averages for a single river should be obtained with time-series measurements that are then flux-weighted to give a yearly average (Livingstone, 1963; Meybeck and Helmer, 1989). Though this is desirable, the number of rivers required to provide large proportions of total water flux renders it impractical.

In many cases, even monthly surveys may not be sufficient (Livingstone, 1963). Fig. 2 shows the 2004 water flux for the Yenisei River (see also Table A.5). The large H_2O pulse associated with the spring freshet accounts for ~40% of the yearly H_2O flux over the course of 1 month (~8% of the year). In the case of large Arctic rivers such as the Yenisei, the freshet must be sampled.

Because of the difficulty of obtaining river samples for specific locations and times, many samples are samples of opportunity. For example, significant tributaries are sometimes assumed to represent the main stem of a river. In this study only one of the exorheic rivers presented in Table 1 is represented by a single major tributary (the Tinguiririca is a tributary of the Rapel).

5.2. Calculation of present-day average Mo and Re concentrations in rivers

Prior estimates of world river Mo and Re averages used sample subsets of three rivers (Amazon, Congo, Maipo) and four rivers (Amazon, Orinoco, Ganges, Brahmaputra), respectively (Bertine and Turekian, 1973; Colodner et al., 1993a). Using global flux and exorheic land area data from Fekete et al. (2002) and Peucker-Ehrenbrink et al. (2007), these subsets account for 22% (Mo) and 24% (Re) of the water flux and 7.6% (Mo) and 6.6% (Re) of exorheic continental area. Though these limited sample sets seemingly necessitate extrapolation to some larger global sub-region, such attempts are meaningless as so few of these regions are characterized. These early investigations extrapolate directly to the global river water flux.

This study analyzes 38 exorheic rivers (Table 1), encompassing 37% of total water runoff and 22% of total exorheic drainage area. This larger more geographically varied sample set allows the regional extrapolation not attempted for previous estimates. In this study, we favor the 19 large-scale drainage regions of Graham et al. (1999) rather than the 14 morphoclimatic zones of Meybeck (1979) or the total continental areas used by Livingstone (1963). The large-scale drainage regions are delineated according to continental runoff into specific regions of the world ocean or large inland seas, and are a useful subdivision of global drainage area as they form part of a river transport algorithm designed for climate modeling (Graham et al., 1999), and because they have been characterized in terms of bedrock geology (Peucker-Ehrenbrink et al., 2007). Table 3 lists the large-scale drainage areas for which data are presented in this study.

The potential for bias introduced by our calculation method is evaluated in Table 4A, using published major elemental concentration data from the compilation of Meybeck and Ragu (1995, ~250 rivers, 60% global H_2O flux, 51% global drainage area). World river averages calculated with this compilation agree well with the published values of Meybeck (1979) and Livingstone (1963). Calculated Meybeck and Ragu (1995) averages also agree well across the different calculation methods for all major anions and cations except K. This generally good agreement is to be expected for a data set accounting for such a large proportion of global totals. Results from the same calculations using data from Table 1 show good agreement with published values of Na, Mg, K, and Cl, but are somewhat higher for Ca, and SO_4. As expected for a much smaller sample set, averages calculated from Table 1 data show larger variations across the different calculation methods. Likewise, published Rb, Sr, and Ba averages (Gaillardet et al., 2003, ~36 rivers, 37% global H_2O, flux, 33% global drainage area), are very similar to those calculated from Table 1 data. Consideration of the river averages calculated for major and minor ions indicates that our sub-sample set is broadly consistent with global river chemistry and can therefore be used to re-calculate the world river average concentrations of Mo and Re. The results of these calculations are presented in Table 4B.

Recalculated Mo and Re world river averages are respectively two and eight times greater than previous estimates (Bertine and Turekian, 1973; Colodner et al., 1993a). Significant changes are not surprising given that the small numbers of rivers evaluated for previous estimates introduces the possibility of significant bias. For example,

despite being only ~17% of the global river H_2O flux, the Amazon accounts for 76% and 85% of total H_2O fluxes used in previous estimates. Because the Amazon has low Mo and Re concentrations, this bias is seen in the world river averages calculated according to different methods in this study (Table 4B). The Amazon represents nearly half of the ~37% of the global river H_2O flux accounted for by the rivers in Table 1; averages calculated by simply scaling to the global H_2O flux are, therefore, lower than those obtained by first scaling to the continental area or large-scale drainage region in which the proportional water flux of the Amazon is kept closer to its global value.

Using modern Mo and Re average river concentrations of 8.0 nmol kg^{-1} and 16.5 pmol kg^{-1} (Table 3B) and a global river H_2O flux of 3.86×10^{16} kg yr^{-1} (Fekete et al., 2002), modern fluxes of these metals to seawater are 3.1×10^8 mol yr^{-1} (Mo) and 6.4×10^5 mol yr^{-1} (Re). In the following sections, we evaluate natural and anthropogenic sources of Mo and Re to world rivers.

5.3. Anthropogenic contributions and the pre-anthropogenic world river average of Re

Industrial production of Mo and Re introduces an anthropogenic component to their modern surface cycles. The potential for a pollutive contribution to Mo was recognized by Bertine and Turekian (1973) and accounts for their decision to estimate an average river concentration based on rivers from the southern hemisphere. Likewise, Manheim and Landergren (1978) used analyses of "pristine" Arctic rivers to estimate that modern Mo fluxes are twice the pre-anthropogenic value. Similarly, Colodner et al. (1995) and Rahaman and Singh (2010) invoke anthropogenic contamination to explain the elevated Re concentrations of rivers draining into the Black Sea and the Gulf of Cambay, respectively.

Anthropogenically-enhanced delivery of Mo and Re to modern oceans is expected on the basis of the high concentrations of these metals in fossil fuels (Bertine and Goldberg, 1971; Poplavko et al., 1974; Duyck et al., 2002; Selby et al., 2005, 2007a), and their presence in fuel processing catalysts (Chang, 1998; Moyse, 2000). Furthermore, the use of Re in brake liners is thought to be the source for high concentrations of Re (up to 10 ng g^{-1}) in road dusts (Meisel and Stotter, 2007).

Table A.8 contains data for precipitation samples from Falmouth, MA, USA. Many of these samples contain non-negligible metal concentrations even after correcting for cyclic sea salt. Concentrations of Mo are consistent with, though generally lower than, those reported for Japanese rain samples (Sugawara et al., 1961). These are the first data for Re in precipitation, and the unexpectedly high concentrations of some samples (e.g. 5.9 pmol Re kg^{-1}) may be evidence of an atmospheric anthropogenic Re component as hypothesized by Chappaz et al. (2008).

Previous studies noted the likelihood of anthropogenic Re contamination in rivers (Colodner et al., 1995; Rahaman and Singh, 2010), and major rivers evaluated for this study (Table 1) may support this, as many known to exhibit anthropogenic effects also have high metal concentrations (Danube, Mississippi, Rhine, Yangtze). Quantifying the effects of anthropogenic contamination is difficult because of wide natural variations and a lack of pre-industrial river samples. Where such samples do exist, they illustrate a large anthropogenic influence on river chemistry (e.g. a 4-fold increase for dissolved SO_4^{2-} and a 13-fold increase for dissolved Cl^- in the Rhine between 1854 and 1981; Zobrist and Stumm, 1981).

Some samples evaluated in this study exhibit unambiguous anthropogenic contamination by virtue of their extremely elevated Re concentrations. The highest river concentration, 1240 pmol Re kg^{-1} for a sample of the South Platte river (Table A.6B), is likely due to evaporative concentration of Re in groundwater used for irrigation. Groundwater irrigation was observed in the area at the time of sampling, and groundwaters exhibit higher concentrations of Re than our world average (Hodge et al., 1996; Leybourne and Cameron, 2008). In addition, a sample of the South Platte from much closer to the headwaters (at 11 Mile Canyon) has a much lower Re concentration (37 pmol kg^{-1}; Table A.6B). Table A.8 contains data for water samples from mining areas (Berkeley Pit from Butte, MT, USA and Kupferschiefer from Mansfeld, Germany). Concentrations of Re in these samples (11,900–37,000 pmol kg^{-1}) are the highest observed for water samples, with enrichment factors of 700–2200 times the average river concentration determined in this study. These samples have concentrations equivalent to or higher than estimates of Re in the crust (Esser and Turekian, 1993; Hauri and Hart, 1997; Peucker-Ehrenbrink and Jahn, 2001; Sun et al., 2003a). Concentrations of Mo in these samples do not display the same level of enrichment; Mansfeld samples show concentrations ranging from 190 to 250 nmol Mo kg^{-1} (23–32 times world river average), Berkeley Pit samples have Mo concentrations of less than 1 nmol kg^{-1} (~0.08 times the world river average). The extremely high Re enrichments but only low to moderately high Mo enrichments in waters associated with mining suggests that Re may be a particularly sensitive tracer of anthropogenic heavy metal contamination.

Given the compelling evidence for anthropogenic Re contamination, it should be quantified in order to determine the pre-anthropogenic river average. The linear relationship observed between Re and SO_4^{2-} in rivers (Section 5.4, Fig. 3; Colodner et al., 1993a; Dalai et al., 2002) allows us to do this. The anthropogenic SO_4^{2-} contribution of world rivers is variably estimated at 28% (Berner, 1971; Meybeck, 1979), 32% (Meybeck, 1988), and 43% (Berner and Berner, 1987). The magnitudes of anthropogenic corrections of global river Re concentration depend on the choice of both average SO_4^{2-} concentration and anthropogenic SO_4^{2-} contribution. Using: (i) SO_4^{2-} river concentration estimates of Meybeck (1979) and Livingstone (1963), and (ii) anthropogenic SO_4^{2-} estimates from the literature (Berner, 1971; Berner and Berner, 1987), (iii) SO_4^{2-} estimates from Table 4A, as well as (iv) pristine river SO_4^{2-} concentration estimates (81.5 μmol SO_4^{2-} kg^{-1}; Meybeck and Helmer, 1989), we obtain pre-anthropogenic world river Re concentrations ranging from 6.5 to 11.9 pmol kg^{-1}.

Our best-estimate for anthropogenically-corrected average river Re concentration is 11.2 pmol kg^{-1}. The estimate

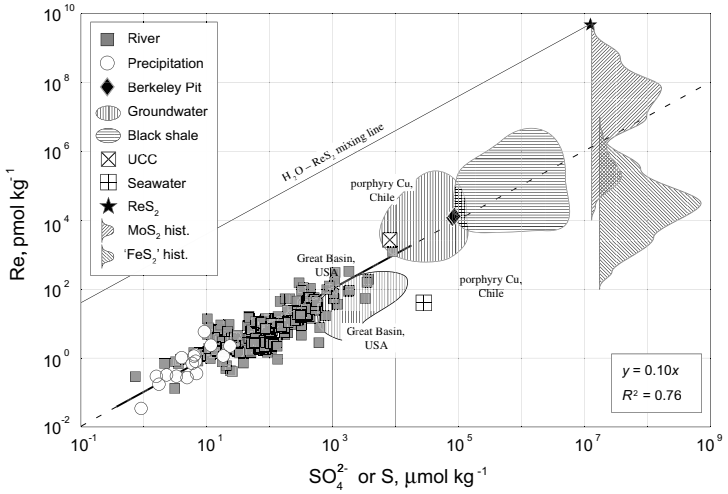

Fig. 3. Rhenium and SO_4^{2-} (or S) in surface waters (Tables 1B, A.5, A.6B, and A.8B), groundwaters, seawater, crustal rocks, and sulfide minerals. A best-fit regression line (forced through the origin) to river data (Tables 1B, A.5, and A.6B) is also plotted, and the resulting slope and coefficient of determination fit parameter (R^2; after Davis, 2002) are provided. Data for groundwaters are from Hodge et al. (1996, Great Basin, USA, $n = 102$) and Leybourne and Cameron (2008, porphyry Cu deposit, Chile, $n = 50$). Data for black shales ($n = 65$) are from Ravizza and Turekian (1989), Cohen et al. (1999), Peucker-Ehrenbrink and Hannigan (2000), Creaser et al. (2002), and Brumsack (2006). Data for the upper continental crust (UCC) are from Mason and Moore (1982) and McLennan (2001). Data for seawater are from Morris and Riley (1966), Anbar et al. (1992), and Colodner et al. (1993a). The range of Re concentrations in MoS_2 ($n = 320$) and Fe-containing sulfides ('FeS_2': $FeS_2 + CuFeS_2 + AsFeS$; $n = 175$) are shown as Log_{10}-scaled histograms. The histograms have bins corresponding to order-of-magnitude ranges in the Re concentration; for example, pyrites with concentrations between 10^4 and 10^5 pmol Re kg^{-1} plot in a single bin; the same is true for concentrations ranging from 10^5 to 10^6 pmol Re kg^{-1}. Note however that the frequency data are linear, rather than Log_{10}-scaled. Data for MoS_2 are from Noddack and Noddack (1931), Fleischer (1959, 1960), Morachevskii and Nechaeva (1960), Terada et al. (1971), McCandless et al. (1993), Markey et al. (1998), Stein et al. (1998, 2001), Selby and Creaser (2001), Barra et al. (2003), Mao et al. (2003), Sun et al. (2003b), Berzina et al. (2005), Zhang et al. (2005), Mao et al. (2006), and Selby et al. (2007b). Data for 'FeS_2' are from Freydier et al. (1997), Brügmann et al. (1998), Cohen et al. (1999), Mathur et al. (1999, 2000, 2005), Stein et al. (2000), Arne et al. (2001), Kirk et al. (2001, 2002), Barra et al. (2003), Hannah et al. (2004), Morelli et al. (2004, 2005, 2007), Zhang et al. (2005), and Liu et al. (2008).

assumes modern SO_4^{2-} and Re world river average concentrations of 120 µmol kg^{-1} and 16.5 pmol kg^{-1} (Meybeck, 1979; Section 5.2), respectively, as well as a pre-industrial SO_4^{2-} estimate of 81.5 µmol kg^{-1} (Meybeck and Helmer, 1989).

Though Mo–SO_4^{2-} in rivers displays a similar degree of linearity to Re–SO_4^{2-} (R^2 of 0.69 and 0.76, Figs. 4 and 3), we hesitate to use SO_4^{2-} as a proxy for Mo pollution because those samples thought to be the most anthropogenically affected on the basis of SO_4^{2-} and Re concentrations do not display concurrent high Mo concentrations (South Platte, Berkeley Pit, Kupferschiefer). We wish to stress that anthropogenic contributions of Mo to world rivers are likely significant, but that using dissolved SO_4^{2-} is not appropriate in correcting for them.

5.4. Continental sources of Mo and Re

Upper continental crustal concentrations for Mo and Re are 1.5 µg g^{-1} and 0.4 ng g^{-1}, respectively (McLennan, 2001). Molybdenum commonly occurs as the sulfide ore mineral molybdenite (MoS_2) though it also forms various oxomolybdate species ($PbMoO_4$, $CaMoO_4$; Evans, 1978), and exhibits high concentrations in common accessory minerals such as magnetite and sphene. In contrast, with the exception of one documented oxide occurrence (Re_2O_7; Petersen et al., 1959), Re is associated exclusively with sulfide minerals, either as an accessory or trace element (FeS_2, $CuFeS_2$, AsFeS, MoS_2; e.g. Fleischer, 1959; Stein et al., 1998; Mathur et al., 2005; Morelli et al., 2005) or, very rarely, as an actual Re mineral (ReS_2, ReS_3, ~$CuReS_4$, ~$Re_4Mo_2CuFeS_{11}$; Capitant et al., 1963; Fleischer, 1963; Morris and Short, 1966; Volborth et al., 1986; Mitchell et al., 1989; Korzhinski et al., 1994; Power et al., 2004). The low crustal abundance, and the rarity with which it forms its own minerals resulted in Re being the last chemical element "discovered" after the isolation of 1 g from ~600 kg of MoS_2 (Noddack et al., 1925; Noddack and Noddack, 1931). A theoretical basis for the association of Mo and Re was later provided by the recognition of similar ionic radii in their geochemically common oxidation states (Whittaker and Muntus, 1970), and has been recently confirmed by synchrotron studies of Re and ^{187}Os in MoS_2 (Takahashi et al., 2007).

Both metals are enriched in modern and ancient reducing sediments (e.g. Koide et al., 1986; Ravizza et al., 1991; Crusius et al., 1996; Morford and Emerson, 1999; Algeo and Lyons, 2006), in which Mo is typically enriched in the diagenetic pyrite rather than the host sediment (Raiswell and Plant, 1980), while Re is present at higher concentrations in the organic matter (Cohen et al., 1999). A comparison of the organic solvent extraction of Mo

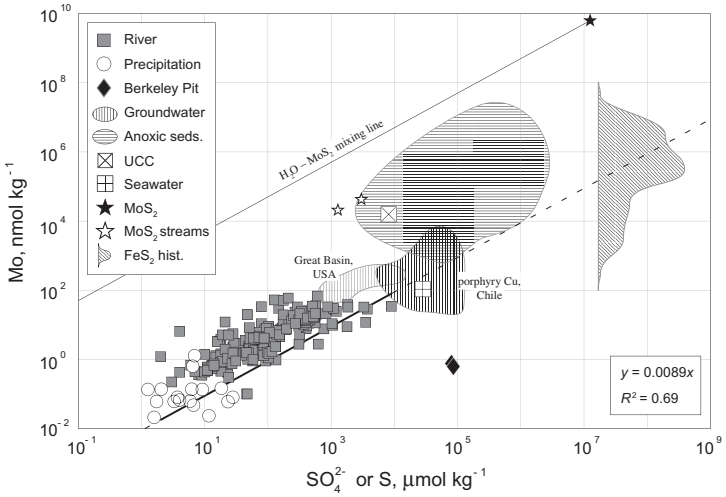

Fig. 4. Molybdenum and SO_4^{2-} (or S) in surface waters (Tables 1B, A.5, A.6B, and A.8B), groundwaters, seawater, crustal rocks, and sulfides (FeS_2, MoS_2). A best-fit regression line (forced through the origin) to river data (Tables 1B, A.5, and A.6B) is also plotted, and the resulting slope and coefficient of determination fit parameter (R^2; after Davis, 2002) are provided. A mixing line between MoS_2 and a hypothetical "pure" water (zero-SO_4^{2-}, zero-Mo) is also shown. Data for groundwaters are from Hodge et al. (1996, Great Basin, USA, $n = 84$) and Leybourne and Cameron (2008, porphyry Cu deposit, Chile, $n = 50$). Data for black shales and Black Sea sediments ("Anoxic seds.," $n = 281$) are from Breger and Schopf (1955), Le Riche (1959), Wedepohl (1964), Vine et al. (1969), Hirst (1974), Pilipchuk and Volkov (1974), Lipinski et al. (2003), Brumsack (2006), Chaillou et al. (2008), and Hetzel et al. (2009). Data for the upper continental crust (UCC) are from Mason and Moore (1982) and McLennan (2001). Data for seawater are from Morris and Riley (1966), Morris (1975), and Collier (1985). Data for streams draining the Climax Mo mine, Colorado ("MoS_2 streams," $n = 2$), are from Kaback and Runnels (1980). Data for the range of Mo concentrations in FeS_2 ($n = 314$) are shown as a smoothed Log_{10}-scaled histogram. The histogram has bins that correspond to an order-of-magnitude range in the Mo concentration; for example, pyrites with concentrations between 10^4 and 10^5 nmol Mo kg^{-1} plot in a single bin; the same is true for concentrations ranging from 10^5 to 10^6 nmol Mo kg^{-1}. Note however that the frequency data are linear, rather than Log_{10}-scaled. Data are from Le Riche (1959), Badalov et al. (1966), Manheim (1972), Manheim and Siems (1972), Volkov and Fomina (1974), Raiswell and Plant (1980), Patterson et al. (1986), Huerta-Diaz and Morse (1992), Huston et al. (1995), Nesheim et al. (1997), Spears et al. (1999), Zhang et al. (2002), Tuttle et al. (2003, 2009), Tribovillard et al. (2008), Large et al. (2009), and Maslennikov et al. (2009).

and Re indicates that a significant proportion of Re, but not Mo, is organically-bound, perhaps as metalloporphyrin species (Miller, 2004).

The association of Re, Mo, and S as sulfides in the crust and the high solubilities of their oxidized species MoO_4^{2-}, ReO_4^-, and SO_4^{2-} implies the effective mobilization of these elements by oxidative weathering and suggests an association in the dissolved phase as seen in Figs. 3 and 4. The linearity of dissolved Re and SO_4^{2-}, previously observed for the individual rivers (Colodner et al., 1993a; Dalai et al., 2002), can now be extended globally.

The Re–SO_4^{2-} relationship in river samples is consistent with precipitation samples, reported groundwater data (Hodge et al., 1996; Leybourne and Cameron, 2008) as well as proposed Re and S concentrations for upper continental crust (UCC) and black shale sources (Fig. 3). In contrast, the Mo–SO_4^{2-} relationship of rivers is consistent with neither the UCC and black shale abundances, nor with the congruent weathering of MoS_2 (Fig. 4). Relative to these presumed sources, rivers exhibit an excess of SO_4^{2-}, a deficit of Mo, or some combination of the two. The differences in the Mo/SO_4^{2-} of rivers, UCC, and MoS_2 are illustrative of the Mo riverine source.

Molybdenum concentrations in FeS_2 (Fig. 4) suggest that modern river concentrations of Mo are consistent with a predominantly pyritic continental source. Sources with higher Mo/S ratios, such as UCC and black shales, must be either less susceptible to weathering or volumetrically unimportant. Likewise, due to the rarity of ReS_2, weathering of this mineral cannot be a significant source of Re to rivers. It should be noted that the observed riverine Re/SO_4^{2-} correlation is consistent with some mixture of MoS_2 and Fe-containing sulfides as the dominant weathering source.

The discrepancy between riverine and UCC Mo/SO_4^{2-} might also be caused by sulfate weathering, but we do not think this is likely. Riverine Re/SO_4^{2-} ratio is consistent with that of UCC, while for Mo/SO_4^{2-} it is much lower. To be consistent with rivers and the UCC, sulfate minerals would need Re concentrations of ~120 ng Re g^{-1} (100-fold higher than the UCC average). Though we have not found published data for Re in sulfate or evaporite minerals, we consider such high concentrations improbable. The corresponding gypsum-anhydrite concentration of Mo, ~6 µg g^{-1}, is of the same order as the UCC Mo average (McLennan, 2001). The range shown by the few published data on sulfate Mo concentrations (10 µg g^{-1} and 60 ng g^{-1}; Manheim and Siems, 1972; Neubert et al., 2011) encompass this value, but we believe the required de-coupling of Re and Mo during weathering and the likelihood of a pyrite Mo source render a significant continental sulfate source unlikely.

Finally, the difference between riverine and UCC Mo/SO_4^{2-} ratios might be due to sorptive loss of weathered

Mo from rivers. This is perhaps best illustrated by Mo concentrations for streams draining the Climax MoS_2 deposit (Colorado, USA, see Fig. 4; Kaback and Runnels, 1980) which show Mo concentrations an order of magnitude below those expected from congruent MoS_2 weathering (Kaback and Runnels, 1980). The isotopic fractionation imparted by Mo adsorption (1‰ amu^{-1} (Barling and Anbar, 2004)) allows us to evaluate this potential sink. Widespread Mo depletion due to Mn-oxide adsorption should result in the enrichment of ^{98}Mo in dissolved river samples, which is consistently observed (Archer and Vance, 2008; Pearce et al., 2010; Scheiderich et al., 2010; Neubert et al., 2011). Assuming an initial dissolved $\delta^{98/95}$ Mo of 0‰ (Siebert et al., 2003) and using a Rayleigh (1896) fractionation model, the observed riverine $\delta^{98/95}Mo$ range of 0–2.4‰ corresponds to 0–55% Mo removal via oxide sorption. However, because riverine Mo/SO_4^{2-} is lower by an order of magnitude or more relative to a UCC or MoS_2 source, Mo loss by sorption to Mn oxides during riverine transport is unable to account for the low Mo/SO_4^{2-} ratio or rivers (see Fig. 4).

5.5. Mo and Re in high temperature hydrothermal fluids from the Manus Basin

Since the discovery of seafloor hydrothermal vents in 1977 (Corliss et al., 1979), characterization of hydrothermal fluids has been important to constrain chemical fluxes to and from seawater (Edmond et al., 1979). Previous studies of high-temperature hydrothermal fluids observe Mo concentrations significantly lower than that of seawater (Trefry et al., 1994; Metz and Trefry, 2000), while lower-temperature (~25 °C) ridge-flank hydrothermal systems have Mo concentrations several times higher than seawater (Wheat et al., 2002). Using these concentrations and hydrothermal water flux estimates (Elderfield and Schultz, 1996), the Mo hydrothermal flux to seawater is estimated at 14% of the previously estimated riverine flux (Wheat et al., 2002). There are no equivalent published Re concentrations for hydrothermal fluids. Laboratory modeling studies of Re in hydrothermal systems (Xiong and Wood, 1999, 2001, 2002) indicate that Re concentrations may be elevated in high-temperature brines due to Cl^--complexation, but that such waters in equilibrium with sulfide minerals could have very low Re concentrations because of sulfide precipitation. Supporting this, high concentrations of Re (10^0–10^2 ng g^{-1}) have been observed in hydrothermal sulfides (Koide et al., 1986; Roy-Barman and Allègre, 1994; Ravizza et al., 1996).

Data for four hydrothermal fluid samples and one bottom seawater sample from the Roman Ruins (RMR) vent site, PACMANUS hydrothermal field, Manus Basin, are presented in Table 2. Fluids were sampled in August and September 2006 during *R/V Melville* cruise MGLN06MV using the ROV *JasonII*. Samples were collected in 755 mL Ti-syringe samplers and extracted immediately after completion of dive operations. Rapidly-precipitating sulfides ("dregs," see Table 2) were collected at sea on a 0.22 μm filter using Milli-Q water; slowly-precipitating sulfides ("bottle filtrate," see Table 2) were isolated on-shore by 0.22 μm filtration. Particulates were removed from filters by dissolution using concentrated Optima Grade HNO_3 (see Craddock et al., 2010 for details).

The sampling of hydrothermal fluids introduces artifacts from the entrainment of chimney particles or ambient seawater, as well as from sulfide mineral precipitation from the temperature and pressure changes experienced during sample collection. Because Mo and Re are susceptible to precipitation as sulfides, reincorporation of these phases with the dissolved phase is crucial in determining metal concentrations for the original fluid. This same tendency to form sulfides may also inflate the concentrations of these metals through addition of chimney fragments.

The sampled fluid mass (assumed to be 750 g) as well as the dregs, and bottle filtrate solution masses used to reconstruct the sampled fluid are presented in Table 2. Concentrations of Mg for these samples (Craddock et al., 2010) are included to allow subtraction of the entrained seawater metal fraction. Samples were vetted using trace element data which indicate no evidence of sample contamination due to incorporation of chimney fragments or loss of precipitated particulates (Craddock et al., 2010).

As seen in Table 2, large proportions of the Mo and Re in these fluids (~81% and ~61%, respectively) are present in the sulfide fractions (dregs + bottle filtrate). The predominance of these metals in the sulfide mineral fraction has already been observed for Mo (Trefry et al., 1994) and is predicted for Re (Xiong and Wood, 2001, 2002). Also, the reconstructed metal concentrations of the fluids as they were sampled (i.e. not Mg-corrected) are all lower than the locally observed or accepted seawater values (Collier, 1985; Anbar et al., 1992), indicating that high-temperature hydrothermal circulation acts as a sink for these metals. In three of four instances, the Re/Mg ratios of these reconstituted fluids are all less than the local seawater value, while the remaining sample has a lower Mo/Mg value. These deficits cannot be the result of Mo and Re scavenging into precipitating sulfides, because it is the reconstituted (fluid + sulfides) values that show the deficit. Assuming that end-member fluid compositions are Mg-free (Seyfried and Mottl, 1982; Seyfried, 1987), these reconstituted samples should nonetheless display Mo and Re concentrations consistent with the Mg concentration of the sampled fluid and seawater metal/Mg ratios. The observed Mo/Mg and Re/Mg values suggest that these high-temperature hydrothermal fluids are not "zero-Mg" and that Mo and Re can be removed more rapidly than Mg during hydrothermal circulation. This explains the large negative Mo concentration observed for sample RMR 2; three of four samples also exhibit negative Re concentrations, but they are likely within uncertainty of zero given the various assumptions made during the reconstruction of the fluid sample concentrations (e.g. an initial fluid mass of 750 g). The RMR 2 Mo concentration of −27 nmol kg^{-1} is far more likely to be significant. We posit that the assumption of zero-Mg in the end-member fluid resulted in a negative Mo concentration for RMR 2 because the Mo/Mg ratio of local bottom water was used in the Mg correction. Negative Mo concentrations in Mg-corrected hydrothermal fluids have been observed in other

studies (Trefry et al., 1994; Metz and Trefry, 2000). Should these fluids all contain Mg, the Mo and Re concentrations reported in Table 2 are all minimum values.

Magnesium-corrected metal concentrations show Re as essentially absent from these fluids, while Mo is present at levels consistent with those reported from other high-temperature vent sites (Trefry et al., 1994; Metz and Trefry, 2000). Assuming the fluids are Mg-free and that Mo and Re concentrations listed in Table 2 are representative of high-temperature hydrothermal fluids (Mo ~22 nmol kg^{-1}, Re ~1.4 pmol kg^{-1}; all negative values assumed to be 0), a high-temperature hydrothermal water flux of 3×10^{13} kg yr^{-1} (Elderfield and Schultz, 1996) results in the removal of 2.6×10^{6} mol Mo yr^{-1} and 1.2×10^{3} mol Re yr^{-1}. These fluxes correspond to approximately 0.4% and 0.1% of the respective modern Mo and pre-anthropogenic Re river fluxes to seawater presented earlier. High-temperature hydrothermal alteration is obviously not a significant source or sink for Mo and Re in seawater.

5.6. Response times and modeling of Mo and Re inventories in seawater

The response time (τ) of a system characterizes its readjustment to equilibrium after a perturbation; for a reservoir with first order sink fluxes it is also called the turnover time or residence time, and is expressed as the ratio of the magnitude of the reservoir to the magnitude of the flux out (M/f_{out}; Rodhe, 1992). The seawater reservoirs are calculated using concentrations of 104 nmol Mo kg^{-1} (Morris, 1975; Collier, 1985), 40 pmol Re kg^{-1} (Anbar et al., 1992; Colodner et al., 1993a, 1995), an oceanic volume of 1.332×10^{21} L (Charette and Smith, 2010), and an average seawater density of 1.028 kg L^{-1} (after Montgomery, 1958 and Millero and Poisson, 1981).

Sinks of oceanic Mo and Re are more difficult to quantify (e.g. Morford and Emerson, 1999), so response times are calculated by assuming steady state and using the fluxes of Mo and Re to seawater. The main source fluxes of Mo to seawater are river water, 3.1×10^{8} mol yr^{-1} (Section 5.2), and low temperature hydrothermal fluids, 2.6×10^{7} mol yr^{-1} (assuming a low temperature hydrothermal Mo flux of 13% of the previous riverine flux estimate, Metz and Trefry, 2000). The major source of Re to seawater is the dissolved river flux, 4.3×10^{5} mol yr^{-1} (pre-anthropogenic, Section 5.3). The low-temperature hydrothermal Re flux cannot be evaluated due to a lack of data; we assume these fluids to be negligible sources of seawater Re. The resulting Mo and Re response times are 4.4×10^{5} yr (τ_{Mo}), and 1.3×10^{5} yr (τ_{Re}, pre-anthropogenic). The τ_{Re} corresponding to the modern anthropogenically-enhanced Re flux is 8.2×10^{4} yr.

The response times presented in this study are significantly shorter than previous estimates (τ_{Mo}, 8.0×10^{5} yr; τ_{Re}, 7.5×10^{5} yr; Colodner et al., 1993a; Morford and Emerson, 1999; see also Section 2). Seawater inventories of both metals are, therefore, more sensitive to changing source or sink fluxes than was previously thought. Previous response times were not only longer, they were also similar to one another (τ_{Re} was 82% of τ_{Mo}), while our data indicate that Re is much more responsive to perturbations than Mo (pre-anthropogenic τ_{Re} is 30% of τ_{Mo}). Fig. 5A shows model results for changing inventories of Mo and Re in seawater due to an increase in the magnitude of the anoxic sink. The model uses first order rate constants calculated assuming steady-state as well as modern and pre-anthropogenic fluxes for Mo and Re respectively (see Appendix). To illustrate the comparative response of these metals to changing source/sink fluxes, we assign a *proportional* anoxic sink flux of 30% for both metals (Morford and Emerson, 1999; Siebert et al., 2003), and a stepwise doubling (210% increase) of the *absolute* anoxic sink fluxes. Under these conditions, the seawater metal inventories of both Mo and Re eventually re-equilibrate to 75% of their modern values, but Re re-equilibrates much more rapidly.

Though differing equilibration times result in varying seawater Re/Mo (after Fig. 5A), the Re/Mo ratio is most often used as an indicator of local redox conditions. Based on analyses of modern depositional environments, Crusius et al. (1996) posit that anoxic sediments exhibit seawater Re/Mo values (0.4 pmol $nmol^{-1}$ or 0.8 ng μg^{-1}) due to quantitative metal removal from the oceanic source, whereas suboxic sediments have higher values due to the more efficient enrichment of Re. However, this also implies that seawater Re/Mo may exhibit secular change due to changing proportions of the various sinks.

Values for Re/Mo of up to 8 pmol $nmol^{-1}$ have been observed in ancient sediments (Turgeon and Brumsack, 2006), so the potential for secular variation is evaluated using a model promoting a rapid increase of seawater Re/Mo. The Re/Mo of seawater increases by enhancing the oxic Mo sink flux, and decreasing the suboxic and anoxic Re fluxes. Oxic sedimentary environments are currently found beneath about 97% of the ocean (Morford and Emerson, 1999), so oxic Mo deposition was only increased by 3%. Because Re is more enriched in suboxic sediments (Crusius et al., 1996), this Re sink flux was removed from the model. Though anoxic sediments represent ~30% of modern oceanic sinks for both Mo and Re (Morford and Emerson, 1999; Siebert et al., 2003), the elimination of these sink fluxes increases seawater Re/Mo; this is also consistent with increased oxic and decreased suboxic deposition as described. Our fully oxic model ocean sees a moderate (~40%) increase in the seawater Mo inventory from the elimination of the anoxic sink (Fig. 5B), but the elimination of essentially all Re sinks results in a steadily increasing Re inventory and Re/Mo ratio (Fig. 5C). The Re/Mo ratio does not reach the elevated values seen in Turgeon and Brumsack (2006, 8 pmol $nmol^{-1}$) until after 3 million years of fully oxic seawater, and even more modest values such as 2 pmol $nmol^{-1}$ (Lipinski et al., 2003) require 750 kyr. After 3 Myr of a fully oxic marine environment, the seawater Re inventory would be ~30 times the modern value (Fig. 5B), and we would expect the corresponding values of Re/C_{org} for reducing sediments to be very high. However Re/C_{org} ratios corresponding to Re/Mo values of 8 pmol $nmol^{-1}$ are only about twice those of Holocene sediments from the Black Sea (97 and 44 nmol mol^{-1}, respectively; Ravizza et al., 1991; Turgeon and Brumsack, 2006). In light of the persistence and specificity of depositional conditions

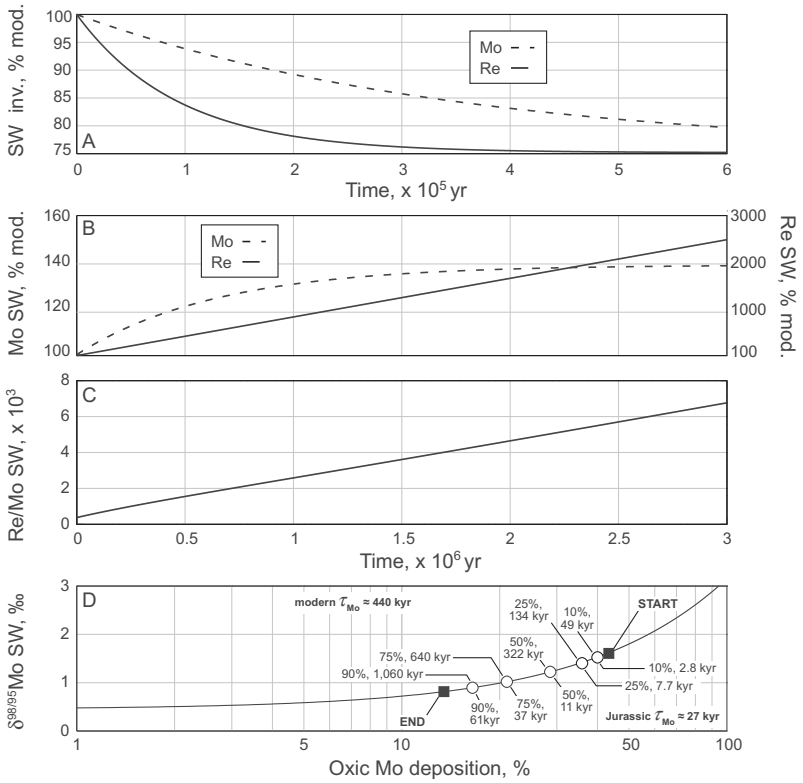

Fig. 5. (A) Response of Mo and Re seawater inventories to a 210% increase in the anoxic metal flux. Seawater metal inventories are expressed as a percentage of the modern value (SW inv., % mod.). (B) Response of Mo and Re seawater inventories to a fully oxidizing ocean (no suboxic, or anoxic sinks). Seawater metal inventories are expressed as a percentage of the modern value (SW inv., % mod.). (C) Response of the Re/Mo seawater ratio to a fully oxidizing ocean. (D) Equilibration times for seawater $\delta^{98/95}$Mo for a deviation of 0.72‰ (1.53–0.81‰), the largest rapid-scale deviation for Jurassic seawater observed by Pearce et al. (2008). Molybdenum isotope re-equilibration was calculated using two values for the Mo response time: the modern value of 440 kyr (this study), and a Jurassic value of 27 kyr calculated by assuming the 0.72‰ deviation represents complete Mo isotopic equilibration, the stratigraphic thickness over which the deviation was observed as related to the total thickness of the *Cleviceras exaratum* ammonite subzone which endured for 1.1 Myr (McArthur et al., 2000), and by assuming constant sedimentation rates over the ammonite subzone (Kemp et al., 2005). $\delta^{98/95}$Mo data are presented against the proportion of oxic Mo deposition after the model formalized by Ling et al. (2005). See text for further discussion.

required to substantially elevate seawater Re concentrations, we argue that the observed Re/Mo variability of ancient sediments is predominantly due to local depositional conditions rather than secular change in the Re/Mo of seawater.

The sensitivity of Mo and Re to differing redox conditions has been exploited not only at the elemental level, but in isotopic studies as well. The fractionation associated with adsorption of Mo to Mn-oxides has been used to comment on the paleoredox state of the global ocean (Siebert et al., 2003; Barling and Anbar, 2004; Pearce et al., 2008), while Re isotope signatures are both redox variable and particularly sensitive to reduction processes (Miller, 2009). The study of Pearce et al. (2008) is particularly valuable as it documents a series of ancient, seemingly rapid $\delta^{98/95}$Mo excursions during the Jurassic. Because the analyzed core has a well understood chronology (McArthur et al., 2000; Kemp et al., 2005; Pearce et al., 2008, see also Fig. 5D), it is possible to estimate that a 0.72‰ change in global seawater $\delta^{98/95}$Mo happened over ~150 kyr. This could not occur today (Siebert et al., 2003) given the modern τ_{Mo} of 4.4×10^5 yr, so by assuming that the 0.72‰ change represents full isotopic equilibration and by comparing with modern Mo isotopic cycling (Fig. 5D), we estimate a Jurassic τ_{Mo} of ~27 kyr. Though isotope studies of Re are only beginning, redox-related Re isotope variability would be even more rapid for a more reducing global ocean such as that of the Jurassic.

6. CONCLUSIONS

We use a set of 38 global rivers encompassing 37% of total water discharge and 25% of exorheic continental drainage area to calculate modern world river average concentrations of 8.0 nmol Mo kg^{-1} and 16.5 pmol Re kg^{-1} by extrapolating to large-scale drainage regions (Graham et al., 1999). Similar calculations produce world river average major cation and Cl^- concentrations consistent with published values (Livingstone, 1963; Meybeck, 1979; Meybeck and Ragu, 1995). Calculated average values of SO_4^{2-} were somewhat higher than published values.

Some samples indicate an anthropogenic component to these new river averages, particularly for Re. Corresponding Mo enrichments for these samples are nonexistent or

Table A.5
River time-series samples, sampling dates, and chemical data for Arctic rivers and Mississippi tributaries. Chemical data are listed to the last significant digit. Where the last significant digit is zero, this is indicated by a decimal point or scientific notation. Uncertainties are as listed in Section 3. Data listed as "b.d." were below the detection limits.

River, date (yr/m/d)	H_2O[a] ($km^3\ d^{-1}$)	Mo ($nmol\ kg^{-1}$)	Re ($pmol\ kg^{-1}$)	Cl ($\mu mol\ kg^{-1}$)	SO_4 ($\mu mol\ kg^{-1}$)	Na ($\mu mol\ kg^{-1}$)	Mg ($\mu mol\ kg^{-1}$)	Ca ($\mu mol\ kg^{-1}$)	K ($\mu mol\ kg^{-1}$)	Rb ($nmol\ kg^{-1}$)	Sr ($nmol\ kg^{-1}$)	Ba ($nmol\ kg^{-1}$)
Kolyma, 2004/06/11	1.56	1.07	3.6	3.0×10^2	101	46	73	212	22	0.9	460	52
Kolyma, 2004/06/15	1.30	1.01	2.7	19	58	42	77	186	17	b.d.	1.0×10^2	43
Kolyma, 2004/06/25	1.01	1.28	2.8	21	86	48	82	250.	14	b.d.	110	35
Kolyma, 2004/07/15	0.617	1.62	2.9	21	98	58	80.	228	14	b.d.	110	40.
Kolyma, 2004/08/10	0.416	1.48	2.6	24	104	63	91	260.	12	b.d.	150	39
Kolyma, 2004/08/25	0.536	1.67	2.6	23	116	60.	91	268	12	b.d.	160	37
Kolyma, 2004/09/23	0.358	2.3	2.2	31	131	70	121	352	11	b.d.	260	42
Lena, 2004/09/04	0.200	4.3	4.6	1610	320	1600	353	660.	18	5.4	1400	140
Lena, 2004/06/05	5.37	2.2	3.0	280.	99	340	233	333	37	60.	600	2.0×10^2
Lena, 2004/06/07	6.69	1.81	3.2	190.	81	250	166	357	20.	7.5	1200	70.
Lena, 2004/08/19	3.07	3.9	2.6	21	52	350	141	356	13	2.9	600	59
Lena, 2004/08/24	2.69	3.7	2.9	290	116	330	150.	361	12	2.1	500	74
Lena, 2004/10/07	2.14	3.4	2.6	290	112	350	168	370.	10.	0.7	500	61
Lena, 2004/10/10	2.26	3.0	2.1	157	83	210	175	393	9	0.62	440	63
Lena, 2007/05/26	2.08	1.32	0.72	120.	38	130	73	288	8	2.2	900	62
Lena, 2007/05/27	3.15	2.9	1.91	390	108	410	191	390.	27	9	900	93
Lena, 2007/05/28	4.94	2.8	2.19	380	103	420	187	385	32	9	800	91
Lena, 2007/05/29	6.22	2.2	1.75	450	87	340	158	310.	28	8	600	77
Lena, 2007/05/30	7.01	2.0	1.71	320	80.	310	149	294	28	9	600	79
Lena, 2007/05/31	7.78	2.0	1.84	310	78	330	149	291	29	9	500	74
Lena, 2007/06/02	8.64	1.9	2.12	250	69	270	143	305	30.	9	500	70.
Lena, 2007/06/02	8.50	1.9	1.91	250	65	260	142	291	29	9	500	76
Lena, 2007/06/04	8.03	1.81	1.96	210	62	230	89	390.	29	8	700	45
Lena, 2007/06/05	9.50	1.55	1.58	190	49	190	126	265	24	7	410	70.
Lena, 2007/06/06	8.99	1.55	1.69	158	46	180	123	278	24	6	500	70.
Lena, 2007/06/08	7.67	1.63	1.51	91	31	130	123	273	24	4.8	320	64
Lena, 2007/06/09	7.49	1.50	1.79	90.	31	120	126	285	23	4.5	320	64
Lena, 2007/06/10	7.38	0.80	0.78	47	17.6	66	93	255	14	2.7	290	60.
Lena, 2007/06/11	7.23	1.45	1.61	79	29	1.0×10^2	139	312	23	4.7	380	69
Ob, 2004/04/05	0.307	5.4	15.9	250	136	250	360.	718	31	10.	1.0×10^3	44
Ob, 2004/06/15	2.98	2.6	12.9	117	85	220	129	354	28	5.0	280	63
Ob, 2004/06/17	2.98	3.0	13.9	110.	85	220	128	360.	29	4.2	320	66
Ob, 2004/07/28	2.25	3.8	1.26	94	62	220	140.	385	32	3.6	380	71
Ob, 2004/08/11	1.37	4.1	11.3	116	59	260	159	411	27	3.5	410	72
Ob, 2004/10/11	0.771	4.6	11.1	140.	75	320	209	565	21	1.9	600	80.
Ob, 2004/10/14	0.829	4.3	10.7	130.	72	320	207	549	20.	3.5	600	79
Ob, 2007/05/29	3.21	0.89	2.09	50.	19	80	49.4	136	13	3.0	80	33
Ob, 2007/05/30	3.20	0.56	1.57	97	12.8	68	21.0	174	13	3.5	1.0×10^3	20.
Ob, 2007/05/31	3.14	0.38	1.26	60.	9.1	60.	35.5	67.8	12	4.2	30.	23

Ob, 2007/06/01	3.14	0.44	1.57	55	10.3	70	39.0	71.5	14	5.6	33	26
Ob, 2007/06/02	3.13	0.60	1.48	67	11.0	55	31.7	75.3	10.	2.7	39	28
Ob, 2007/06/03	3.11	0.36	1.41	102	7.7	63	32.9	53.6	13	4.7	15	22
Ob, 2007/06/04	3.08	0.35	1.14	54	8.6	62	32.8	57.5	11	3.4	17	25
Ob, 2007/06/05	3.03	0.53	2.1	31	13.1	66	40.6	73.2	12	3.3	30.	31
Ob, 2007/06/06	3.02	0.44	0.82	79	7.2	55	30.4	53.8	10.	3.8	12	22
Ob, 2007/06/07	3.02	0.53	1.30	34	11.4	65	37.2	68.9	12	5.1	31	27
Ob, 2007/06/08	3.02	0.43	4.9	48	10.3	50.	32.4	55.6	10.	3.0	16	26
Ob, 2007/06/09	3.01	0.47	7.5	53	10.8	58	33.5	58.8	10.	3.0	18	30.
Ob, 2007/06/10	3.00	0.74	2.1	30.	14.1	46	36.5	82.8	9	1.9	39	34
Ob, 2007/06/11	3.00	1.06	3.1	80.	23	90	52.8	124	14	3.5	90	33
Ob, 2007/06/12	3.01	0.22	0.78	20.	3.2	31	17.1	40.7	5.2	1.1	b.d.	21
Ob, 2007/06/13	3.01	0.61	1.35	51	12.7	70	38.2	80.3	11	3.5	42	26
Ob, 2007/06/14	3.01	0.47	1.9	63	10.8	70	37.8	65.3	10.	4.2	30.	31
Ob, 2007/06/15	3.08	0.49	0.96	36	11.4	80	39.6	84.3	13	b.d.	30.	16
Ob, 2007/06/16	3.10	0.67	1.60	40.	13.9	70	41.0	92.3	10.	3.2	45	29
Ob, 2007/06/17	3.11	0.68	1.43	25	6.2	40.	24.1	57.9	5.8	1.3	9	23
Yenisei, 2004/03/19	0.638	6.7	9.9	3.0×10^2	144	380	214	664	20.	1.9	1400	82
Yenisei, 2004/06/14	8.51	1.53	3.0	44	28	6.0	61.5	164	0.56	b.d.	150	28
Yenisei, 2004/06/16	8.16	0.74	4.1	61	27	90	60.8	164	8	b.d.	140	27
Yenisei, 2004/06/18	7.83	0.88	4.6	63	31	1.0×10^2	75	168	9	1.6	180	34
Yenisei, 2004/08/25	1.57	6.0	10.3	280	105	360	195	506	16	2.6	1.0×10^3	65
Yenisei, 2004/10/01	1.72	3.9	7.1	180	87	3.0×10^2	163	454	12	0.7	800	54
Yenisei, 2004/10/02	1.67	4.1	7.1	250	87	3.0×10^2	162	442	11	0.32	800	50.
Mackenzie, 2004/03/24	0.327	9.3	16.8	380	410	5.0×10^2	374	847	24	4.4	1400	260
Mackenzie, 2004/06/17	1.58	9.0	14.9	143	310	240	307	817	20.	5.4	1200	250
Mackenzie, 2004/06/22	1.50	2.8	15.5	130.	310	220	308	766	22	9	1.0×10^3	3.0×10^2
Mackenzie, 2004/07/13	1.08	10.4	16.2	181	360	290	336	868	20.	4.7	1100	240
Mackenzie, 2004/08/04	0.07	11.5	20.	210	4.0×10^2	330	369	903	22	5.6	1400	250
Mackenzie, 2004/08/25	0.754	13.0	15.8	240	410	370	412	980	28	19	1600	380
Mackenzie, 2004/08/09	0.758	13.2	15.7	260	430	4.0×10^2	402	950	26	11	1600	310
Yukon, 2004/04/07	0.1138	13.6	12.0	79	280	160	332	818	33	13	700	140
Yukon, 2004/05/26	1.282	5.1	8.1	43	152	80	187	593	25	8	410	160
Yukon, 2004/06/15	1.563	7.6	10.8	42	2.0×10^2	70	212	717	27	10.	320	2.0×10^2
Yukon, 2004/06/29	1.258	19	12.3	69	250	1.0×10^2	258	812	29	12	500	220
Yukon, 2004/07/19	0.8685	13.9	15.6	74	310	140	322	800	54	35	700	260
Yukon, 2004/08/18	0.8172	14.6	17.5	66	4.0×10^2	160	391	828	63	55	900	410
Yukon, 2004/09/22	0.4942	14.1	17.8	85	390	160	381	970	42	19	900	250
Arkansas, 2004/02/12	0.112	6.6	19	1110	280	–	–	–	–	–	–	–
Arkansas, 2004/04/15	0.122	9.3	27	1390	370	–	–	–	–	–	–	–
Arkansas, 2004/07/17	0.205	9.3	22	1350	320	–	–	–	–	–	–	–
Arkansas, 2004/11/13	0.113	12.4	17.7	1520	310	–	–	–	–	–	–	–

(*continued on next page*)

Table A.5 (*continued*)

River, date (yr/m/d)	H_2O[a] ($km^3\ d^{-1}$)	Mo ($nmol\ kg^{-1}$)	Re ($pmol\ kg^{-1}$)	Cl ($\mu mol\ kg^{-1}$)	SO_4 ($\mu mol\ kg^{-1}$)	Na ($\mu mol\ kg^{-1}$)	Mg ($\mu mol\ kg^{-1}$)	Ca ($\mu mol\ kg^{-1}$)	K ($\mu mol\ kg^{-1}$)	Rb ($nmol\ kg^{-1}$)	Sr ($nmol\ kg^{-1}$)	Ba ($nmol\ kg^{-1}$)
Missouri, 2004/02/10	0.0785	21	96	770	810	–	–	–	–	–	–	–
Missouri, 2004/04/14	0.0785	30.	164	610	1.10×10^3	–	–	–	–	–	–	–
Missouri, 2004/07/12	0.204	33	123	6.0×10^2	880	–	–	–	–	–	–	–
Missouri, 2004/11/12	0.153	15.6	57	360	420	–	–	–	–	–	–	–
Ohio, 2004/02/12	2.14	16.0	25	710	540	–	–	–	–	–	–	–
Ohio, 2004/04/14	0.484	17.0	34	590	520	–	–	–	–	–	–	–
Ohio, 2004/07/17	0.519	35	51	480	5.0×10^2	–	–	–	–	–	–	–
Ohio, 2004/11/13	0.776	21	43	500	560	–	–	–	–	–	–	–
Upper Mississippi, 2004/02/11	0.0864	26	106	1.20×10^3	440	–	–	–	–	–	–	–
Upper Mississippi, 2004/04/14	0.409	11.0	45	570	270	–	–	–	–	–	–	–
Upper Mississippi, 2004/07/16	0.416	25	112	550	340	–	–	–	–	–	–	–
Upper Mississippi, 2004/11/12	0.294	21	91	6.0×10^2	320	–	–	–	–	–	–	–

[a] Water flux data for Arctic rivers were taken from the University of New Hampshire's (UNH) Arctic Regional, Integrated Hydrological Monitoring System (RIMS) website available at http://rims.unh.edu/.

Kolyma River at Kolymskoye; Station Code 1802; Lat, Lon: 68.7500, 002.6458
Lena River at Kusur; Station Code 3821; Lat, Lon: 66.7664, 123.3967
Ob River at Salekhard; Station Code 11801; Lat, Lon: 66.5414, 066.4722
Yenisei River at Igarka; Station Code 9803; Lat, Lon: 67.4344, 086.3908
Mackenzie River at Arctic Red River; Station Code 10LC014; Lat, Lon: 67.4521, −133.7389
Yukon River at Pilot Station AK; Station Code 15565447; Lat, Lon: 61.9486, −162.9077

Water flux data for Mississippi tributaries were taken from the United States Geological Survey (USGS) National Water Information System (NWIS) available at http://waterdata.usgs.gov/nwis/.

Arkansas River at Murray Dam near Little Rock AK; Station ID 07263450; Lat, Lon: 33.9878, −091.3625
Missouri River at Hermann MO; Station ID 06934500; Lat, Lon: 38.5610, −092.0092
Ohio River at Metropolis IL; Station ID 03611500; Lat, Lon: 37.0010, −089.1638
Upper Mississippi River at Grafton IL; Station ID 05587450; Lat, Lon: 38.8827, −090.1882

Table A.6A
Sample, sampling date and location information for tributary and exorheic river samples. Entries in bold are those samples used to calculate values presented in Table 1 and/or were calculated from data presented in Table A.5.

River	Date (yr/m/d)	Large-scale drainage region	Continent	Country	Latitude (decimal °)	Longitude (decimal °)
Kolyma	**2004**	**1**	**Asia**	**Russia**	**68.7500**	**002.6458**
Lena	**2004**	**1**	**Asia**	**Russia**	**66.7664**	**123.3967**
Ob	**2004**	**1**	**Asia**	**Russia**	**66.5414**	**066.4722**
Ob (Yamal Nemetz)	2006/11/09	1	Asia	Russia	71.4833	071.8000
Yenisei	**2004**	**1**	**Asia**	**Russia**	**67.4344**	**086.3908**
Mackenzie	**2004**	**2**	**North America**	**Canada**	**67.4521**	**−133.7389**
Mackenzie	2007/07/04	2	North America	Canada	68.4659	−134.1283
Big Vulcan Lake	2000/08/23	3	North America	USA	42.1877	−123.9845
Bighorn	2005/05/19	3	North America	USA	45.6446	−107.6585
Bitterroot	2005/05/20	3	North America	USA	46.6323	−114.0663
Blackfoot	2005/05/20	3	North America	USA	46.8737	−113.8855
Boulder Lake	2000/??/??	3	North America	USA	42.8558	−109.6228
Coffee Creek	2000/08/26	3	North America	USA	41.1235	−122.8203
Connecticut	**2004/07/08**	**3**	**North America**	**USA**	**41.4853**	**−072.5142**
Connecticut	**2004/07/08**	**3**	**North America**	**USA**	**41.4853**	**−072.5142**
Connecticut	**2004/07/08**	**3**	**North America**	**USA**	**41.4816**	**−072.5066**
Connecticut	**2004/07/08**	**3**	**North America**	**USA**	**41.4816**	**−072.5066**
Croton outlet (Hudson watershed)	2004/09/29	3	North America	USA	41.2069	−073.8217
Croton outlet (Hudson watershed)	2004/09/29	3	North America	USA	41.2069	−073.8217
Esophus Creek	2004/09/30	3	North America	USA	42.0677	−074.3057
Esophus Creek	2004/09/30	3	North America	USA	42.0677	−074.3057
Freemont Lake	2000/??/??	3	North America	USA	42.9453	−109.7951
Freemont Lake	2000/??/??	3	North America	USA	42.9453	−109.7951
Gallatin	2005/05/25	3	North America	USA	45.9342	−111.4931
Half Moon Lake	2000/??/??	3	North America	USA	42.9365	−109.7620
Hot spring	2005/05/20	3	North America	USA	46.1372	−112.8918
Housatonic	**2004/07/08**	**3**	**North America**	**USA**	**41.3852**	**−073.1724**
Housatonic	**2004/07/08**	**3**	**North America**	**USA**	**41.3852**	**−073.1724**
Hudson	2004/09/30	3	North America	USA	41.8321	−073.9415
Hudson	2004/09/30	3	North America	USA	41.8321	−073.9415
Hudson	**2006/06/06**	**3**	**North America**	**USA**	**42.7611**	**−037.6847**
Jefferson	2005/05/25	3	North America	USA	45.8973	−111.6104
Lake George	2004/10/01	3	North America	USA	43.4200	−073.7086
Madison	2005/05/25	3	North America	USA	45.9009	−111.5261
Mississippi	**2004**	**3**	**North America**	**USA**	**29.9208**	**−090.1353**
Mississippi	2005/05/27	3	North America	USA	45.3257	−093.8239
Mississippi (at New Orleans)	2004/04	3	North America	USA	29.9566	−090.0615
Missouri	2005/05/18	3	North America	USA	41.3569	−095.9502
Missouri	2005/05/19	3	North America	USA	45.9399	−111.4904
Missouri	2005/05/25	3	North America	USA	46.7591	−100.8410
Mohawk	2004/09/30	3	North America	USA	42.8484	−074.0143
North Platte	2005/05/18	3	North America	USA	41.3171	−102.1262
Pine Creek	2000/??/??	3	North America	USA	43.0349	−109.7648
Platte	2005/05/18	3	North America	USA	41.0148	−096.1580
Platte, North Channel	2005/05/18	3	North America	USA	41.0194	−100.3715
Platte, South Channel	2005/05/18	3	North America	USA	41.0545	−102.0732
pond (Hudson watershed)	2004/09/30	3	North America	USA	41.9240	−073.9109
Powder, North Fork	2005/05/19	3	North America	USA	43.7726	−106.7103
Powder, South Fork	2005/05/19	3	North America	USA	43.7084	−106.6036
Runoff from Josephine Peridotite	2000/08/23	3	North America	USA	42.1836	−123.9933
St. Croix	2005/05/27	3	North America	USA	44.9613	−092.7737
St. Lawrence (Contrecœur)	**2008/05/18**	**3**	**North America**	**Canada**	**45.8586**	**−073.2397**
St. Lawrence (Coteau du Lac)	2008/05/18	3	North America	Canada	45.2798	−074.1782
Schaeffer's Creek	2004/10/01	3	North America	USA	43.2861	−073.8217
Shoharie Creek	2004/09/30	3	North America	USA	42.5999	−074.3360
Shoharie Creek	2004/09/30	3	North America	USA	42.5999	−074.3360

(*continued on next page*)

Table A.6A (*continued*)

River	Date (yr/m/d)	Large-scale drainage region	Continent	Country	Latitude (decimal °)	Longitude (decimal °)
Silver Bow Creek	2005/05/25	3	North America	USA	45.9957	−112.5388
Soda Lake	2000/??/??	3	North America	USA	42.9558	−109.8528
South Platte (11 Mile Canyon)	2008/16/17	3	North America	USA	38.9268	−105.4251
Stream (Clay City)	2000/01/12	3	North America	USA	37.8733	−083.9478
Upper Cabin Meadow Lake	2000/08/25	3	North America	USA	41.3398	−122.5884
Upper Hudson	2004/10/01	3	North America	USA	43.2873	−073.8262
Upper Hudson	2004/10/01	3	North America	USA	43.2873	−073.8262
Willow Lake	2000/??/??	3	North America	USA	42.9911	−109.8993
Yellowstone	2005/05/19	3	North America	USA	45.5977	−110.5658
Yellowstone	2005/05/25	3	North America	USA	47.2814	−104.5248
Fnjóskà	2006/06	4	Europe	Iceland	65.7131	−017.8994
Homsà	2006/06/07	4	Europe	Iceland	63.6500	−018.3917
Lake Mývatn	2006/06/03	4	Europe	Iceland	65.6396	−016.9159
Ölfusà	**2006/06**	**4**	**Europe**	**Iceland**	**63.9383**	**−021.0083**
Rhine	**2007/08/25**	**4**	**Europe**	**Germany**	**50.9481**	**006.9714**
River (Blönduòs)	2006/06/02	4	Europe	Iceland	65.6582	−020.2855
Skaftarskà	2006/06/07	4	Europe	Iceland	63.7939	−018.0399
Þjórsà	**2006/06**	**4**	**Europe**	**Iceland**	**63.9300**	**−020.6400**
Amazon (Macapá)	**2005/03/25**	**5**	**South America**	**Brazil**	**00.0333**	**−051.0500**
Negro	2005/03/28	5	South America	Brazil	−03.1500	−060.0333
Solimões	2005/03/27	5	South America	Brazil	03.2500	−060.0000
Orange	**2005/08**	**6**	**Africa**	**Namibia**	**−28.0833**	**016.8917**
Zaire/Congo	**????/??/??**	**6**	**Africa**	**Democratic Republic of Congo**	**−04.2990**	**015.2777**
Brahmaputra	**2006/06/21**	**8**	**Asia**	**Bangladesh**	**25.2833**	**089.6333**
Brahmaputra	**2006/06/23**	**8**	**Asia**	**Bangladesh**	**24.9014**	**089.5794**
Brahmaputra	**2007/08/16**	**8**	**Asia**	**Bangladesh**	**24.4084**	**089.7986**
Ganga	**2007/08/17**	**8**	**Asia**	**Bangladesh**	**24.0553**	**089.0314**
Indus	**2007/02/28**	**8**	**Asia**	**Pakistan**	**25.4422**	**068.3164**
Karnali	2007/08/09	8	Asia	Nepal	28.3689	081.2035
Kosi	2007/08/16	8	Asia	Nepal	26.8481	087.1514
Meghna	**2006/01/18**	**8**	**Asia**	**Bangladesh**	**23.5993**	**090.6102**
Narayani	2007/08/08	8	Asia	Nepal	27.7030	084.4266
Padma	2007/08/19	8	Asia	Bangladesh	23.4598	090.2540
Trisuli	2007/08/12	8	Asia	Nepal	27.8100	084.8433
Yarlung	2006/??/??	8	Asia	China	29.3472	090.1447
Fly	**1993/??/??**	**9**	**Oceania**	**Papua New Guinea**	**−08.4150**	**143.2422**
Fly	**1993/??/??**	**9**	**Oceania**	**Papua New Guinea**	**−08.4150**	**143.2422**
Fly	**1993/??/??**	**9**	**Oceania**	**Papua New Guinea**	**−08.4150**	**143.2422**
Fly	**1993/??/??**	**9**	**Oceania**	**Papua New Guinea**	**−08.4150**	**143.2422**
Kikori	**1993/??/??**	**9**	**Oceania**	**Papua New Guinea**	**−07.6809**	**144.8354**
Kikori	**1993/??/??**	**9**	**Oceania**	**Papua New Guinea**	**−07.6809**	**144.8354**
Pearl	**2006/06/18**	**9**	**Asia**	**China**	**26.1153**	**113.2681**
Purari	**1993/??/??**	**9**	**Oceania**	**Papua New Guinea**	**−07.7017**	**143.8317**
Purari	**1993/??/??**	**9**	**Oceania**	**Papua New Guinea**	**−07.7017**	**143.8317**
Red	**2006/06/11**	**9**	**Asia**	**Vietnam**	**21.0544**	**105.8472**
Sepik	**1993/??/??**	**9**	**Oceania**	**Papua New Guinea**	**−03.9051**	**144.5403**
Waiahole Stream	2006/08/24	9	Oceania	USA	21.4816	−157.8487
Waimea Falls Pond	2006/08/24	9	Oceania	USA	21.6306	−158.0440
Waimea Reservoir	2006/08/24	9	Oceania	USA	21.4908	−158.0260
Yangtze	**2007/??/??**	**9**	**Asia**	**China**	**30.2872**	**111.5264**
Blackwater	2006/09/18	10	North America	Canada	53.2875	−123.1422
Copper	**2008/08/22**	**10**	**North America**	**USA**	**60.4453**	**−145.0667**
Fraser	**2006/08/22**	**10**	**North America**	**Canada**	**49.5056**	**−121.4142**
Fraser	**2006/08/08**	**10**	**North America**	**Canada**	**49.5633**	**−121.4028**
Fraser	2006/09/19	10	North America	Canada	–	–

Table A.6A (*continued*)

River	Date (yr/m/d)	Large-scale drainage region	Continent	Country	Latitude (decimal °)	Longitude (decimal °)
Harrison	2006/07/27	10	North America	Canada	49.2372	−121.9633
Nechako	2006/09/11	10	North America	Canada	–	–
Nechako	2006/09/19	10	North America	Canada	–	–
North Thompson	2006/07/14	10	North America	Canada	–	–
Quesnel	2006/09/18	10	North America	Canada	52.9833	−122.4822
Thompson	2006/09/05	10	North America	Canada	50.3492	−121.3906
Upper Fraser	2006/07/15	10	North America	Canada		
Yukon	**2004/??/??**	**10**	**North America**	**USA**	**61.9486**	**−162.9077**
Andalién	**2004/02/12**	**11**	**South America**	**Chile**	**−36.8019**	**−073.9667**
Andalién	**2004/02/12**	**11**	**South America**	**Chile**	**−35.6844**	**−071.1106**
Biobío	**2004/02/12**	**11**	**South America**	**Chile**	**−36.8088**	**−073.0979**
Biobío	**2004/02/12**	**11**	**South America**	**Chile**	**−36.8688**	**−073.0445**
Biobío	**2006/08/24**	**11**	**South America**	**Chile**	**−36.8393**	**−073.0514**
Biobío	**2007/02/01**	**11**	**South America**	**Chile**	**−37.5991**	**−072.2781**
River (Fundación Huinay)	2007/02/06	11	South America	Chile	−42.3811	−072.4155
Itata	**2006/06/28**	**11**	**South America**	**Chile**	**−36.6242**	**−072.4816**
Itata	**2007/02/02**	**11**	**South America**	**Chile**	**−36.4666**	**−072.6916**
Maipo	**2007/01/29**	**11**	**South America**	**Chile**	**−33.6288**	**−070.3548**
Maule	**2007/01/31**	**11**	**South America**	**Chile**	**−35.7236**	**−071.1763**
River (Pichicolo)	2007/02/06	11	South America	Chile	−41.9749	−072.5530
Tinguiririca	**2006/09/16**	**11**	**South America**	**Chile**	**−34.6125**	**−070.9818**
Tinguiririca	**2007/01/30**	**11**	**South America**	**Chile**	**−34.6789**	**−070.8739**
Toltén	**2006/06/25**	**11**	**South America**	**Chile**	**−39.0109**	**−073.0818**
Toltén	**2007/02/03**	**11**	**South America**	**Chile**	**−38.9772**	**−072.6364**
Toltén	**2007/02/04**	**11**	**South America**	**Chile**	**−39.2743**	**−072.2301**
Pelorus	2006/12/20	12	Oceania	New Zealand	−41.2988	173.5734
Danube (Budapest)	**2007/05/04**	**16**	**Europe**	**Hungary**	**47.5000**	**019.0500**
Danube (Passau)	2007/05/02	16	Europe	Germany	48.5767	013.4567
Danube (Regensburg)	2007/05/02	16	Europe	Germany	49.0214	012.1219
Danube (Ulm)	2007/05/02	16	Europe	Germany	48.3950	009.9928
Danube (Vienna)	2007/05/04	16	Europe	Austria	48.2261	016.4086
Iller (Wiblinger)	2007/05/02	16	Europe	Germany	–	–
Inn (Schärding)	2007/05/02	16	Europe	Germany	48.4572	013.4267
March (Angern an der March)	2007/05/03	16	Europe	Austria	–	–
Regen (Regensburg)	2007/05/02	16	Europe	Germany	49.0211	012.1219
Tisza (Szeged)	2007/05/04	16	Europe	Hungary	46.2494	020.1533

only moderate, indicating that Re might be a sensitive indicator of anthropogenic metal contamination. We estimate that 32% of Re is of anthropogenic origin, and that the pre-industrial river average Re concentration is 11.2 pmol kg^{-1}.

On the basis of a relationship between Re and SO_4^{2-} (Colodner et al., 1993a; Dalai et al., 2002), the source of Re to rivers is dominated by sulfide mineral and black shale weathering. A similar relationship between Mo and SO_4^{2-} implies that pyrite weathering is the principal source of Mo to rivers.

This study also presents the first data on Re in hydrothermal fluids. High temperature hydrothermal fluids from the Manus Basin show Mo and Re concentrations much lower than those of ambient seawater. In particular, Re was essentially absent in calculated end-member hydrothermal fluids. The data indicate that Mo and Re can be removed from seawater more effectively than Mg during high-temperature hydrothermal alteration. High temperature hydrothermal fluids represent a negligible sink in comparison to the river source of these metals.

Using the new world river Mo and pre-anthropogenic river Re concentration averages, we have recalculated modern Mo and Re response times (τ_{Mo}, preindustrial τ_{Re}) as 4.4×10^5 yr and 1.3×10^5 yr, respectively. These response times indicate that Mo and especially Re will re-equilibrate more quickly to changing metal sources and sinks than was previously thought (Colodner et al., 1993a; Morford and Emerson, 1999). Furthermore, our enhanced understanding of Mo and Re sources to seawater can help evaluate increasingly common paleoredox proxies such as Re/Mo and $\delta^{98/95}$Mo.

ACKNOWLEDGMENTS

We would like to acknowledge financial support from NSF grants EAR 0519387 (B.P.-E.), OPP 0229302 (PARTNERS), OPP 0519840 (Student Partners), and OPP 0732522 (Arctic-GRO), as well as the WHOI Academic Programs Office (C.A.M.), and the WHOI Arctic Research Initiative. We also acknowledge support from Tulane-Xavier Center for Bioenvironmental Research and LEAG (NOAA-USGS) program (F.M.), as

Table A.6B
Sample ID and chemical data for tributary and exorheic river samples. Entries in bold are those samples used to calculate values presented in Table 1 and/or were calculated from data presented in Table A.5. Data listed as "b.d." were below the detection limits.

River	Mo (nmol kg^{-1})	Re (pmol kg^{-1})	Cl (μmol kg^{-1})	SO_4 (μmol kg^{-1})	Na (μmol kg^{-1})	Mg (μmol kg^{-1})	Ca (μmol kg^{-1})	K (μmol kg^{-1})	Rb (nmol kg^{-1})	Sr (nmol kg^{-1})	Ba (nmol kg^{-1})
Kolyma	**1.47**	**2.9**	**92**	**100.**	**55**	**87**	**250**	**15**	**b.d.**	**230**	**42**
Lena	**3.0**	**2.9**	**260**	**96**	**370**	**178**	**380**	**16**	**5.3**	**800**	**78**
Ob	**3.9**	**12.5**	**135**	**83**	**3.0×10^2**	**185**	**460**	**28**	**4.7**	**500**	**66**
Ob (Yamal Nemetz)	2.8	7.6	1770	630	230	185	430	23	3.6	430	84
Yenisei	**3.5**	**6.5**	**168**	**73**	**2.0×10^2**	**131**	**360**	**10**	**1.0**	**600**	**49**
Mackenzie	**10.1**	**16.2**	**240**	**380**	**350**	**359**	**870**	**23**	**7**	**1300**	**270**
Mackenzie	11.1	14.1	440	440	70	414	1.0×10^3	3.5	0.7	2100	280
Big Vulcan Lake	b.d.	0.13	25	3.1	33	333	10.	0.36	b.d.	b.d.	17
Bighorn	28	1.9×10^2	430	3700	4700	1350	1400	140	31	8000	240
Bitterroot	3.8	1.23	14.4	18.5	90	41.6	140	23	3.5	70	60.
Blackfoot	2.9	2.9	14.6	40	7	285	580	1.7	0.28	170	620
Boulder Lake	0.67	4.0	6.6	13.2	28	14.9	56	10	3.1	b.d.	28
Coffee Creek	3.3	3.4	190	16.5	180	444	540	4.0	b.d.	32	20
Connecticut	**7.8**	**14.9**	–	–	–	–	–	–	–	–	–
Connecticut	**7.7**	**14.8**	–	–	–	–	–	–	–	–	–
Connecticut	**7.9**	**13.9**	–	–	–	–	–	–	–	–	–
Connecticut	**7.9**	**13.9**	–	–	–	–	–	–	–	–	–
Croton outlet (Hudson watershed)	4.8	5.7	1520	108	1.0×10^3	293	6.0×10^2	52	9	120	120
Croton outlet (Hudson watershed)	4.9	5.7	1530	108	1100	296	6.0×10^2	53	10.	110	131
Esophus Creek	0.12	3.7	66	46	90	35.7	120	8	b.d.	b.d.	48
Esophus Creek	0.14	3.7	66	47	90	36.3	120	8	b.d.	b.d.	47
Freemont Lake	1.17	6.6	8.5	15.2	25	11.4	51	10.	2.9	b.d.	28
Freemont Lake	1.29	6.7	9.4	15.1	25	11.9	52	9	1.9	b.d.	26
Gallatin	7.6	11.3	51	159	230	300	730	44	10.	680	181
Half Moon Lake	0.65	4.1	7.2	13.3	25	15.1	52	8	0.8	b.d.	27
hot spring	33	8.2	13.3	79	90	174	610	25	13	170	83
Housatonic	**5.4**	**6.7**	–	–	–	–	–	–	–	–	–
Housatonic	**5.6**	**6.6**	–	–	–	–	–	–	–	–	–
Hudson	5.7	7.7	520	126	450	173	640	38	3.8	350	88
Hudson	4.2	7.7	520	127	460	173	660	38	3.3	340	99
Hudson	**3.2**	**7.2**	**660**	**124**	–	–	–	–	–	–	–
Jefferson	23	17.8	91	268	340	291	640	55	11	500	170
Lake George	1.34	5.2	470	80.	410	102	350	13	b.d.	38	36
Madison	52	10.2	510	126	1500	197	5.0×10^2	1.0×10^2	190	3.0×10^2	107
Mississippi	**21**	**57**	**640**	**510**	–	–	–	–	–	–	–
Mississippi	8.2	13.5	250	96	2.0×10^2	521	1.0×10^3	36	9	180	230
Mississippi (New Orleans)	13.9	29	760	460	660	478	1.0×10^3	47	2.3	600	260
Missouri	39	3.3×10^2	490	1810	2100	1140	1600	140	20.	3600	310

Missouri	14.0	14.9	110.	220	4.0×10^2	364	870	60	26	800	2.0×10^2
Missouri	32	93	320	1840	2900	860	1200	1.0×10^2	18	2900	270
Mohawk	4.5	7.8	5.0×10^2	153	480	207	860	31	b.d.	800	104
North Platte	27	3.0×10^2	370	1090	2400	483	930	230	61	3.0×10^3	6.0×10^2
Pine Creek	1.44	3.6	5.6	17.5	24	11.7	75	11	2.7	b.d.	33
Platte	36	220	280	–	900	633	1600	247	21	2400	730
Platte, North Channel	30.	44	77	147	610	276	1400	239	49	1900	1.0×10^3
Platte, South Channel	34	1240	3.0×10^3	9.0×10^3	9000	2460	3900	483	62	14000	190
Pond (Hudson watershed)	1.47	6.2	710	111	6.0×10^2	134	870	33	b.d.	5.0×10^2	77
Powder, North Fork	8.8	87	102	1780	1800	960	1600	55	7.9	4200	220
Powder, South Fork	7.6	16.8	250	770	650	472	1.0×10^3	39	5.0	2500	100
Runoff from Josephine Peridotite	b.d.	0.29	34	4.8	44	424	10.	2.6	b.d.	b.d.	24
St. Croix	3.5	8.6	157	44	120	306	550	24	4.5	26	81
St. Lawrence (Contrecœur)	**12.1**	**24**	**580**	**230**	**520**	**292**	**810**	**35**	**10.**	**1200**	**109**
St. Lawrence (Coteau du Lac)	12.3	17.8	610	240	520	300.	850	36	9	1200	106
Schaeffer's Creek	2.57	4.7	181	65	160	370.	520	12	b.d.	b.d.	b.d.
Shoharie Creek	0.87	4.3	180.	57	190	62.3	280	21	b.d.	12	57
Shoharie Creek	0.94	4.3	181	57	190	62.4	290	20	b.d.	6.7	56
Silver Bow Creek	82	40.	250	–	390	262	710	61	7	1100	160
Soda Lake	4.9	42	6300	–	3100	6150	2100	3200	130	1300	86
South Platte (11 Mile Canyon)	19	37	1220	580	1500	611	1.0×10^3	51	7	2600	190
Stream (Clay City)	11.7	157	660	3500	2.0×10^2	395	1.0×10^3	110	29	500	93
Upper Cabin Meadow Lake	b.d.	0.29	2.1	0.73	4.8	342	9.4	0.9	b.d.	b.d.	160
Upper Hudson	1.24	3.9	3.0×10^2	48	240	54.7	210	8	2.3	23	37
Upper Hudson	1.02	3.9	3.0×10^2	48	240	54.3	210	8	2.2	18	45
Willow Lake	0.43	9.4	20.	23	47	21.3	73	13	1.6	15	42
Yellowstone	7.0	4.1	75	97	310	136	280	52	64	220	80
Yellowstone	11.3	29	94	560	700	339	650	46	12	900	150
Fnjóskà	0.42	0.92	33	3.8	65	20.4	45	2.2	b.d.	b.d.	12.6
Homsà	2.3	1.83	78	28	220	72.6	110	12	1.2	b.d.	20
Lake Mývatn	10.6	11.2	–	–	1200	203	340	60	34	b.d.	16
Ölfusà	**1.04**	**1.74**	**153**	**24**	$\mathbf{3.0 \times 10^2}$	**56.5**	$\mathbf{1.0 \times 10^2}$	**12**	**2.0**	**b.d.**	**3300**
Rhine	**10.8**	**57**	**1210**	**390**	**800**	**356**	**1500**	**80**	**24**	**2600**	**190**
River (Blönduòs)	1.32	1.39	93	18	15	89	110	10	b.d.	b.d.	18
Skaftarskà	1.76	3.6	87	79	270	78	160	9	b.d.	b.d.	b.d.
Þjórsà	**4.1**	**4.1**	**86**	**61**	**320**	**63.1**	$\mathbf{1.0 \times 10^2}$	**11**	**b.d.**	**b.d.**	**13.4**
Amazon (Macapá)	**0.89**	**1.83**	–	**92**	$\mathbf{1.0 \times 10^2}$	**67.8**	**160**	**30**	**40.**	**150**	**240**
Negro	0.15	b.d.	–	–	17	3.1	5.9	4.9	9	b.d.	336
Solimões	0.65	3.0	–	23	130	91	310	29	41	390	330
Orange	**24**	**37**	**2800**	**1210**	**3600**	**1090**	$\mathbf{1.0 \times 10^3}$	**60**	**1.9**	$\mathbf{2.0 \times 10^3}$	**330**
Zaire/Congo	**0.45**	**3.0**	**36**	**17.9**	**90**	**62.1**	**523**	**39**	**31**	**17**	**79**
Brahmaputra	**13.2**	**5.4**	**44**	**190**	**220**	**253**	$\mathbf{7.0 \times 10^2}$	**60**	**28**	**600**	**99**
Brahmaputra	**11.8**	**4.8**	**44**	**174**	**210**	**263**	$\mathbf{7.0 \times 10^2}$	**59**	**26**	**600**	**95**
Brahmaputra	**8.4**	**3.0**	**40**	**102**	**93**	**134**	**450**	**57**	**27**	**240**	**73**

(*continued on next page*)

Table A.6B (*continued*)

River	Mo (nmol kg^{-1})	Re (pmol kg^{-1})	Cl (μmol kg^{-1})	SO_4 (μmol kg^{-1})	Na (μmol kg^{-1})	Mg (μmol kg^{-1})	Ca (μmol kg^{-1})	K (μmol kg^{-1})	Rb (nmol kg^{-1})	Sr (nmol kg^{-1})	Ba (nmol kg^{-1})
Ganga	**10.7**	**3.9**	**67**	**79**	**220**	**193**	**620**	**80**	**14**	**450**	**140**
Indus	**36**	**29**	**840**	**570**	**530**	**472**	**1100**	**110**	**7**	**6000**	**3.0×10^3**
Karnali	6.4	4.1	50	103	70	215	580	37	38	430	120
Kosi	5.7	2.2	31	62	70	60.7	3.0×10^2	34	37	1.0×10^2	20
Meghna	**2.4**	**1.40**	**80**	**50.**	**240**	**146**	**240**	**31**	**17**	**170**	**45**
Narayani	8.1	5.4	59	170	80	288	620	46	54	4.0×10^2	102
Padma	9.1	3.3	42	103	90	127	470	58	16	290	79
Trisuli	5.4	1.74	33	69	70	74	370	33	45	180	24
Yarlung	18.6	8.39	230	320	580	254	910	42	93	1500	58
Fly	**51**	**52**	–	**175**	**330**	**134**	**870**	**23**	**6.1**	**800**	**69**
Fly	**59**	**52**	–	**210**	**320**	**131**	**870**	**23**	**7**	**900**	**70.**
Fly	**61**	**53**	–	–	**1.0×10^2**	**105**	**870**	**18**	**5.1**	**900**	**70.**
Fly	**62**	**52**	–	–	**90**	**104**	**860**	**16**	**4.4**	**1.0×10^3**	**71**
Kikori	**3.2**	**9.1**	–	**16.7**	**60.**	**284**	**1.0×10^3**	**10.**	**6.3**	**1.0×10^3**	**41**
Kikori	**3.8**	**9.4**	–	–	**50.**	**278**	**1.0×10^3**	**9**	**4.5**	**800**	**34**
Pearl	**12.3**	**10.9**	**220**	**174**	**320**	**65.8**	**410**	**80**	**1.0×10^2**	**170**	**90.**
Purari	**3.9**	**3.4**	–	**88**	**800**	**282**	**730**	**42**	**14**	**700**	**54**
Purari	**4.0**	**3.4**	–	**87**	**700**	**274**	**7.0×10^2**	**38**	**12**	**700**	**52**
Red	**6.7**	**13.4**	**68**	**126**	**170**	**217.5**	**740**	**44**	**29**	**1100**	**190**
Sepik	**2.0**	**1.64**	–	–	**610**	**243**	**250**	**24**	**14**	**180**	**89**
Waiahole Stream	0.80	0.49	320	20.	370	177	150	14	4.6	90	34
Waimea Falls Pond	0.30	0.42	420	24	350	115	65	20	1.9	16	20.
Waimea Reservoir	0.79	0.41	360	26	330	70.9	46	15	2.2	b.d.	30.
Yangtze	**15.8**	**55**	**310**	**420**	**440**	**373**	**7.0×10^2**	**47**	**15**	**1700**	**240**
Blackwater	12.0	6.0	12	21	280	427.7	460	60	19	500	44
Copper	**14.4**	**9.3**	**53**	**210**	**1.0×10^2**	**107**	**520**	**36**	**11**	**220**	**85**
Fraser	**7.8**	**5.3**	**22**	**101**	**1.0×10^2**	**128**	**410**	**16**	**10.**	**5.0×10^3**	**57**
Fraser	**7.9**	**5.2**	**20.**	**94**	**90**	**124**	**410**	**16**	**10.**	**5.0×10^3**	**56**
Fraser	3.0	2.9	8.7	131	43	202	620	12	12	800	64
Harrison	8.3	4.5	15	51	49	24.8	160	14	5.6	80	49
Nechako	20	16.3	17	47	1.0×10^2	166	380	17	3.5	390	79
Nechako	19	14.6	12	47	1.0×10^2	167	370	17	3.3	410	80.
North Thompson	6.0	2.6	8.3	73	39	62.7	290	17	17	367	36
Quesnel	3.4	3.0	3.3	82	36	100	5.0×10^2	10	4.5	900	36
Thompson	7.1	4.3	19	88	80	85	320	21	16	427	46
Upper Fraser	0.96	0.92	8.0	134	23	200.	430	4.4	b.d.	800	57
Yukon	**12.0**	**13.4**	**65**	**280**	**120**	**297**	**790**	**38**	**21**	**600**	**230**
Andalién[a]	**1.35**	**13.7**	**162**	**10.**	**580**	**177**	**360**	**43**	**17**	**900**	**70.**
Andalién	**1.16**	**0.67**	**144**	**2.1**	**450**	**147**	**290**	**30.**	**12**	**800**	**43**

Biobío[a]	**2.1**	**5.7**	**88**	**50.**	**250**	**113**	**220**	**27**	**22**	**320**	**19**
Biobío	**2.0**	**6.7**	**89**	**51**	**240**	**99**	**180**	**25**	**23**	**270**	**18**
Biobío	**2.2**	**3.5**	**67**	**28**	**180**	**93**	**140**	**22**	**17**	**230**	**16**
Biobío	**2.9**	**3.8**	**136**	**59**	**210**	**93**	**210**	**28**	**32**	**26**	**20**
river (Fundación Huinay)	5.0	3.8	28	24	47	45	250	160	20.	1700	4.4
Itata[a]	**2.9**	**1.60**	**53**	**29**	**190**	**94**	**120**	**22**	**24**	**280**	**20.**
Itata	**6.5**	**0.69**	**330**	**3.5**	**900**	**472**	**430**	**46**	**3.0**	**1500**	**126**
Maipo[a]	**33**	**53**	**2500**	**3300**	**2900**	**387**	**3700**	**70**	**70**	**1.0×10^4**	**86**
Maule[a]	**19**	**7.4**	**190**	**174**	**360**	**129**	**280**	**33**	**46**	**440**	**22**
River at Pichicolo	68	2.78	2800	610	3800	34	320	21	40	210	8.7
Tinguiririca[a]	**12.6**	**17.0**	**161**	**370**	**330**	**110.**	**540**	**26**	**39**	**800**	**25**
Tinguiririca	**16.3**	**24**	**117**	**540**	**240**	**114**	**470**	**31**	**43**	**600**	**21**
Toltén	**3.3**	**1.55**	**40.**	**15.6**	**140**	**55.6**	**1.0×10^3**	**19**	**17**	**140**	**14**
Toltén[a]	**5.5**	**2.2**	**49**	**28**	**2.0×10^2**	**75**	**130**	**25**	**23**	**160**	**24**
Toltén	**5.1**	**1.88**	**35**	**19**	**160**	**66.4**	**120**	**22**	**22**	**180**	**12.5**
Pelorus	1.9	0.59	85	21	140	105	160	8	b.d.	70	20
Danube (Budapest)	**10.8**	**74**	**1830**	**1030**	**2.0×10^3**	**1.20×10^3**	**1900**	**160**	**32**	**3300**	**4.0×10^3**
Danube (Passau)	14.4	35	790	330	70	670.	1300	7	1.7	1600	150
Danube (Regensburg)	18.5	43	790	360	800	660.	940	80	20	1500	150
Danube (Ulm)	33	152	1030	290	700	512	1.0×10^3	60	8	1500	160
Danube (Vienna)	11.8	21	5.0×10^2	320	540	498	1100	57	23	1500	108
March (Angern an der March)	9.6	52	1030	1050	1200	750	1600	170	30	2200	210
Iller (Wiblinger)	7.2	24	72	190	470	603	830	50.	3.5	2600	210
Inn (Schärding)	13.0	13.9	280	240	3.0×10^2	381	910	40	21	1400	85
Regen (Regensburg)	2.3	12.7	6.0×10^2	132	490	189	520	56	23	310	88
Tisza (Szeged)	7.8	22	1190	4.0×10^2	1500	360.	1100	74	17	1200	130.

[a] Data for some Chilean rivers originally published in Fiege et al. (2009).

Table A.7
Pearson product-moment correlation coefficients (r; after Davis, 2002) values for dissolved chemical pairs for samples used in this study. Note that the distributions of all individual chemical species are indistinguishable from normal at the 95% level (after Student, 1908). The value of r_{Ba-Cl} is denoted 'n.s.' indicating it is not significant at the 95% level.

	Mo	Re	Cl	SO_4	Na	Mg	K	Ca	Rb	Sr	Ba
Mo	1										
Re	0.35	1									
Cl	0.22	0.09	1								
SO_4	0.41	0.88	0.08	1							
Na	0.40	0.77	0.15	0.85	1						
Mg	0.18	0.42	0.17	0.79	0.60	1					
K	0.48	0.62	0.20	0.75	0.69	0.61	1				
Ca	0.07	0.19	0.16	0.76	0.36	0.91	0.36	1			
Rb	0.29	0.20	0.07	0.26	0.35	0.39	0.44	0.33	1		
Sr	0.32	0.65	0.17	0.86	0.80	0.79	0.61	0.83	0.61	1	
Ba	0.12	0.11	n.s.	0.09	0.12	0.10	0.04	0.19	0.04	0.29	1

well as the Carl and Pancha Peterson Endowed Fund for Support of [WHOI] Summer Student Fellows (B.W.). We would like to thank Tracy Atwood, current and former members of the WHOI Plasma Mass Spectrometry Facility: Lary Ball, Scot Birdwhistell, Jerzy Blusztajn, and Dave Schneider, as well as the members of the Seewald Lab (WHOI): Eoghan Reeves, Jeff Seewald, and Sean Sylva for their analytical assistance. This work would not have been possible without the generous assistance of many friends and collaborators who provided us with water samples: Bridget Bergquist, Peter Clift, Paul Craddock, Ted Duaime, Ricardo Figueroa, Jérôme Gaillardet, Valier Galy, Rocky Geyer, Liviu Giosan, Jaime Hills, Max Holmes, Matt Jackson, Tom Lough, Francis Alexander Macdonald, Candace Martin, Daniel Montluçon, Petra Ehrenbrink, Greg Ravizza, Laura Robinson, Olivier Rouxel, Andrew Schroth, Michael Schubert, Jeff Seewald, Ken Sims, Anna Skuládóttir, Meg Tivey, Rhian Waller, Nadine Zimmer, Yan Zheng. We also thank Ed Sholkovitz for his suggestion to process water by syringe-filtration, and Carl Petersen for encouraging us to investigate anthropogenic Re contamination. We would like to thank the associate editor, Tim Shaw, as well as three anonymous reviewers whose comments significantly improved this manuscript.

APPENDIX A. TABLES A.5, A.6, A.7, A.8

APPENDIX B. MODELING SEAWATER INVENTORIES OF MOLYBDENUM AND RHENIUM

We evaluate the implications of our new Mo and Re world river averages by considering a model that makes four assumptions: (1) the modern ocean is at steady-state with respect to Mo and pre-anthropogenic Re, (2) the riverine fluxes of Mo and Re (pre-anthropogenic) remain constant with time, (3) oxic and anoxic sink fluxes of these metals out of seawater are first order, and (4) the magnitude of these sink fluxes has varied with time (Siebert et al., 2003; Arnold et al., 2004; Pearce et al., 2008).

The inputs of the model are (A) the modern seawater Mo and Re inventories, (B) modern riverine Mo and pre-anthropogenic riverine Re fluxes to seawater, (C) and oxic and anoxic fluxes of Mo and Re from seawater that are used to determine first order flux rate constants for these metals.

(A) The inventories of Mo and Re in modern seawater are

$$\mathrm{Mo_{SW}} = 1.45 \times 10^{14}\ \mathrm{mol} \qquad \mathrm{Re_{SW}} = 5.40 \times 10^{10}\ \mathrm{mol}$$

Using Mo as an example :

$$\begin{aligned}\mathrm{Mo_{SW}} &= \frac{\mathrm{nmol\ Mo}}{\mathrm{L_{SW}}} * \mathrm{volume_{SW}} \\ &= 107\ \frac{\mathrm{nmol\ Mo}}{\mathrm{L_{SW}}} * 1.35 \times 10^{21}\ \mathrm{L_{SW}} \\ &= 1.45 \times 10^{14}\ \mathrm{mol}\end{aligned}$$

(B) The river water (RW) fluxes of Mo and Re to seawater (in) are

$$f\mathrm{Mo_{in}} = 3.09 \times 10^{8}\ \frac{\mathrm{mol}}{\mathrm{yr}} \qquad f\mathrm{Re_{in}} = 4.32 \times 10^{5}\ \frac{\mathrm{mol}}{\mathrm{yr}}$$

Using Mo as an example :

$$\begin{aligned}f\mathrm{Mo_{in}} &= \frac{\mathrm{nmol\ Mo}}{\mathrm{kg_{RW}}} * f\mathrm{H_2O_{RW}} \\ &= 8.0 \frac{\mathrm{nmol\ Mo}}{\mathrm{kg_{RW}}} * 3.86 \times 10^{16}\ \frac{\mathrm{kg}}{\mathrm{yr}} \\ &= 3.09 \times 10^{8}\ \frac{\mathrm{mol}}{\mathrm{yr}}\end{aligned}$$

(C) Oxic (ox) and anoxic (anox) fluxes of Mo and Re from seawater (out) are set at proportions of 0.7 and 0.3 of the flux in. This is based on the Mo isotope work of Siebert et al. (2003); though equivalent proportions are not known for Re, they are also set to 0.7 (oxic) and 0.3 (anoxic) in order to comparatively illustrate the temporal response of these two metals.

$$f\mathrm{Mo_{out\ ox}} = 2.16 \times 10^{8}\ \frac{\mathrm{mol}}{\mathrm{yr}} \quad f\mathrm{Re_{out\ ox}} = 3.03 \times 10^{5}\ \frac{\mathrm{mol}}{\mathrm{yr}}$$

$$f\mathrm{Mo_{out\ anox}} = 9.26 \times 10^{7}\ \frac{\mathrm{mol}}{\mathrm{yr}} \quad f\mathrm{Re_{out\ anox}} = 1.30 \times 10^{5}\ \frac{\mathrm{mol}}{\mathrm{yr}}$$

If fluxes from seawater are first-order (assumption 3), we can solve for the constants of Mo and Re oxic and anoxic flux rates. For example, for $k_{\mathrm{Mo\ out\ ox}}$:

$$\frac{d\mathrm{Mo_{SW}}}{dt}\mathrm{Mo\ out\ ox} = -k_{\mathrm{Mo\ out\ ox}}\ \mathrm{Mo_{SW}}$$

Table A.8
Chemical data for precipitation and mine water samples. Chemical data are listed to the last significant digit. Where the last significant digit is zero, this is indicated by a decimal point or scientific notation. Uncertainties are as listed in Section 3. Data listed as "b.d." were below the detection limits.

Sample	Mo (nmol kg^{-1})	Re (pmol kg^{-1})	Cl (μmol kg^{-1})	SO_4 (μmol kg^{-1})	Na (μmol kg^{-1})	Mg (μmol kg^{-1})	Ca (μmol kg^{-1})	K (μmol kg^{-1})	Rb (nmol kg^{-1})	Sr (nmol kg^{-1})	Ba (nmol kg^{-1})
Precipitation, Falmouth, MA[a]											
2004/09/18	0.080	1.41	103	33	80	10.6	7.1	4.6	b.d.	b.d.	43
2004/09/18	0.080	0.91	23	4.9	4.3	2.20	4.6	1.4	b.d.	b.d.	b.d.
2004/10/15	0.047	0.81	26	8.0	b.d.	2.97	7.5	3.9	b.d.	b.d.	20
2004/12/01	0.64	1.25	204	17.0	140	19.4	7.6	5.6	b.d.	b.d.	16
2004/12/10	0.062	0.70	26	7.2	b.d.	2.79	5.8	b.d.	b.d.	b.d.	33
2004/12/26	0.021	0.29	16.4	2.4	b.d.	1.64	7.1	b.d.	b.d.	b.d.	44
2005/01/06	0.067	1.03	9.8	4.5	b.d.	0.98	4.1	b.d.	b.d.	b.d.	71
2005/01/24	0.061	0.173	57	4.7	23	5.63	5.8	b.d.	b.d.	b.d.	19
2005/02/14	0.147	1.15	9.8	19	b.d.	1.19	5.3	b.d.	b.d.	b.d.	25
2005/02/16	0.135	5.9	440	32	320	39.9	25	19	12	b.d.	21
2005/02/21	0.136	1.13	31	7.9	7	3.31	3.7	b.d.	b.d.	b.d.	35
2005/02/21	b.d.	0.57	14	3.7	b.d.	1.82	3.9	b.d.	b.d.	b.d.	b.d.
2005/02/24–25	0.135	5.9	14	2.0	b.d.	2.54	6.6	b.d.	b.d.	b.d.	b.d.
2005/02/28	0.136	1.13	20	3.1	b.d.	2.53	4.7	b.d.	b.d.	b.d.	28
2005/03/??	0.061	0.30	71	7.0	36	6.87	8.1	1.6	b.d.	b.d.	48
2005/04/15–2005/05/10	0.023	2.4	95	16.6	65	9.1	8.8	3.1	b.d.	b.d.	22
2005/07/08	1.28	0.35	19	7.9	b.d.	1.73	8.0	0.7	b.d.	b.d.	20.
2005/09/16	b.d.	0.034	1.83	1.00	b.d.	0.425	4.3	b.d.	b.d.	b.d.	100.
2005/09/24	b.d.	0.27	71	8.5	46	7.16	6.6	3.5	b.d.	b.d.	69
2005/09/29	0.060	2.2	360	42	280	35.4	21	b.d.	10	b.d.	17
Mine waters											
Berkeley Pit, surface	0.76	11,900	710	8.0×10^4	6.7	268	11,000	90	590	b.d.	930
Berkeley Pit, −76 m	0.62	1.31×10^4	550	86,000	5.1	132	15,000	2.6	270	b.d.	410
Mansfeld 1	220	14,400	–	–	43	4330	16,000	7.0×10^2	470	19,000	120
Mansfeld 2	250	37,100	–	–	2400	4650	14,000	7.0×10^2	570	33,000	150
Mansfeld 3	190	16,200	–	–	2.0×10^4	7070	2.0×10^4	1200	800	14,000	170

[a] Data for precipitation samples are the only ones corrected that have been corrected for cyclic sea salt.

Sampling locations Lat, Lon:
Falmouth, MA, USA: 41.5605, −070.6154
Berkeley Pit, MT, USA: 46.0167, −112.5060
Mansfeld, Germany: 51.5941, −011.4547

the solution to which at time t is

$$\mathrm{Mo_{SW}} = \mathrm{Mo_{SW\ 0}} * e^{-k_{\mathrm{Mo\ out\ ox}} t}$$

The oxic sink flux of Mo out of the oceans over a given time-period is

$$f\mathrm{Mo_{out\ ox}} = \mathrm{Mo_{SW\ 0}}\left(1 - e^{-k_{\mathrm{Mo\ out\ ox}} t}\right)$$

allowing us to solve for k. For example, over the course of 1 yr:

$$\begin{aligned} k_{\mathrm{Mo\ out\ ox}} &= -\log_e\left(1 - \frac{f\mathrm{Mo_{out}}}{\mathrm{Mo_{SW\ 0}}}\right) * \frac{1}{t} \\ &= -\log_e\left(1 - \frac{2.16 \times 10^8\ \mathrm{mol}}{1.45 \times 10^{14}\ \mathrm{mol}}\right) * \frac{1}{1\ \mathrm{yr}} \\ &= 1.490 \times 10^{-6}\ \mathrm{yr}^{-1} \end{aligned}$$

The four flux constants are

$$k_{\mathrm{Mo\ out\ ox}} = 1.490 \times 10^{-6}\ \mathrm{yr}^{-1} \quad k_{\mathrm{Re\ out\ ox}} = 5.611 \times 10^{-6}\ \mathrm{yr}^{-1}$$
$$k_{\mathrm{Mo\ out\ anox}} = 6.386 \times 10^{-7}\ \mathrm{yr}^{-1} \quad k_{\mathrm{Re\ out\ anox}} = 2.407 \times 10^{-7}\ \mathrm{yr}^{-1}$$

A box model for temporal changes in Mo and Re seawater inventories resulting from changing anoxic fluxes can now be constructed.

For a given year (i), using Mo as an example, the metal inventory of seawater is given by,

$$\mathrm{Mo_{SW}}(i) = \mathrm{Mo_{SW}}(i-1) + f\mathrm{Mo_{in}} - f\mathrm{Mo_{out}},$$

where $f\mathrm{Mo_{in}}$ and $f\mathrm{Mo_{out}}$ are metal fluxes into and out of seawater given by,

$$f\mathrm{Mo_{in}} = \frac{\mathrm{nmol\ Mo}}{\mathrm{kg_{RW}}} * f\mathrm{H_2O_{RW}}$$

and

$$\begin{aligned} f\mathrm{Mo_{out}} &= f\mathrm{Mo_{out\ ox}} + f\mathrm{Mo_{out\ anox}} \\ &= \left(\mathrm{Mo_{SW}}(i-1) * \left(1 - e^{-k_{\mathrm{Mo\ out\ ox}} * (i-(i-1))}\right)\right) \\ &\quad + \left(\mathrm{Mo_{SW}}(i-1) * \left(1 - e^{-k_{\mathrm{Mo\ out\ anox}} * i-(i-1)}\right)\right) \end{aligned}$$

and $\mathrm{Mo_{SW}}(i-1)$ refers to inventory of the previous year.

Note that the model presented above only considers oxic and anoxic fluxes. However, it is easily modified to incorporate suboxic fluxes through the addition of another term (e.g. $f\mathrm{Mo_{out\ subox}} = \mathrm{Mo_{SW}}(i-1) * (1 - e^{-k_{\mathrm{Mo\ out\ subox}} * (i-(i-1))})$).

REFERENCES

Algeo T. J. and Lyons T. W. (2006) Mo–total organic carbon covariation in modern anoxic marine environments: implications for analysis of paleoredox and paleohydrographic conditions. *Paleoceanography* **21**, doi:10.1029/2004PA001112.

Anbar A. D., Creaser R. A., Papanastassiou D. A. and Wasserburg G. J. (1992) Rhenium in seawater: confirmation of generally conservative behavior. *Geochim. Cosmochim. Acta* **56**, 4099–4103.

Archer C. and Vance D. (2008) The isotopic signature of the global riverine molybdenum flux and anoxia in the ancient oceans. *Nat. Geosci.* **1**, 597–600.

Arne D. C., Bierlein F. P., Morgan J. W. and Stein H. J. (2001) Re–Os dating of sulfides associated with gold mineralization in central Victoria, Australia. *Econ. Geol.* **96**, 1455–1459.

Arnold G. L., Anbar A. D., Barling J. and Lyons T. W. (2004) Molybdenum isotope evidence for widespread anoxia in mid-Proterozoic oceans. *Science* **304**, 87–90.

Badalov S. T., Basitova S. M., Godunova L. I. and Shodiev F. Sh. (1966) Geochemistry of rhenium and molybdenum in the endogenetic sulfide deposits of middle Asia. *Geochem. Int.* **1**, 64–68.

Barling J. and Anbar A. D. (2004) Molybdenum isotope fractionation during adsorption by manganese oxides. *Earth Planet. Sci. Lett.* **217**, 315–329.

Barra F., Ruiz J., Mathur R. and Titley S. (2003) A Re–Os study of sulfide minerals from the Bagdad porphyry Cu–Mo deposit, northern Arizona, USA. *Miner. Deposita* **38**, 585–596.

Berner R. A. (1971) Worldwide sulfur pollution of rivers. *J. Geophys. Res.* **76**, 6597–6600.

Berner R. A. and Berner E. K. (1987) *The Global Water Cycle*. Prentice-Hall.

Berner R. A. and Raiswell R. (1983) Burial of organic carbon and pyrite sulfur in sediments over Phanerozoic time: a new story. *Geochim. Cosmochim. Acta* **47**, 855–862.

Bertine K. K. and Goldberg E. D. (1971) Fossil fuel combustion and the major sedimentary cycle. *Science* **173**, 233–235.

Bertine K. K. and Turekian K. K. (1973) Molybdenum in marine deposits. *Geochim. Cosmochim. Acta* **37**, 1415–1434.

Berzina A. N., Sotnikov V. I., Economou-Eliopoulos M. and Eliopoulos D. G. (2005) Distribution of rhenium in molybdenite from porphyry Cu–Mo and Mo–Cu deposits of Russia (Siberia) and Mongolia. *Ore Geol. Rev.* **26**, 91–113.

Breger I. A. and Schopf J. M. (1955) Germanium and uranium in coalified wood from upper Devonian black shale. *Geochim. Cosmochim. Acta* **7**, 287–293.

Brookins D. G. (1986) Rhenium as analog for fissiogenic technetium: Eh–pH diagram (25 °C, 1 bar) constraints. *Appl. Geochem.* **1**, 513–517.

Brügmann G. E., Birck J. L., Herzig P. M. and Hofmann A. W. (1998) Os isotopic composition and Os and Re distribution in the active mound of the TAG hydrothermal system, Mid-Atlantic Ridge. *Proc. Ocean Drill. Program, Part B: Sci. Results* **158**, 91–100.

Brumsack H.-J. (2006) The trace metal content of recent organic carbon-rich sediments: implications for Cretaceous black shale formation. *Palaeogeogr. Palaeoclimatol. Palaeoecol.* **232**, 344–361.

Calvert S. E. and Pederson T. F. (1993) Geochemistry of recent oxic and anoxic marine sediments: implications for the geological record. *Mar. Geol.* **113**, 67–88.

Capitant M., Francotte J., Picot P. and Troly G. (1963) Hautes teneurs en rhénium dans une molybdénite de Kipushi. *C. R. Acad. Sci.* **257**, 3443–3444.

Chaillou G., Schäfer J., Blanc G. and Anschutz P. (2008) Mobility of Mo, U, As, and Sb within modern turbidites. *Mar. Geol.* **254**, 171–179.

Chang T. (1998) Regeneration industry helps refiners control costs, limit liabilities. *Oil Gas J.* **96**, 49–54.

Chappaz A., Gobeil C. and Tessier A. (2008) Sequestration mechanisms and anthropogenic inputs of rhenium in sediments from Eastern Canada lakes. *Geochim. Cosmochim. Acta* **72**, 6027–6036.

Charette M. A. and Smith W. H. F. (2010) The volume of Earth's ocean. *Oceanography* **23**, 112–114.

Cohen A. S., Coe A. L., Bartlett J. M. and Hawkesworth C. J. (1999) Precise Re–Os ages of organic-rich mudrocks and the Os isotopic composition of Jurassic seawater. *Earth Planet. Sci. Lett.* **167**, 159–173.

Collier R. W. (1985) Molybdenum in the Northeast Pacific Ocean. *Limnol. Oceanogr.* **30**, 1351–1354.

Colodner D., Edmond J. and Boyle E. (1995) Rhenium in the Black Sea: comparison with molybdenum and uranium. *Earth Planet. Sci. Lett.* **131**, 1–15.

Colodner D., Sachs J., Ravizza G., Turekian K., Edmond J. and Boyle E. (1993a) The geochemical cycle of rhenium: a reconnaissance. *Earth Planet. Sci. Lett.* **117**, 205–221.

Colodner D. C., Boyle E. A. and Edmond J. M. (1993b) Determination of rhenium and platinum in natural waters and sediments, and iridium in sediments by flow injection isotope dilution inductively coupled plasma mass spectrometry. *Anal. Chem.* **65**, 1419–1425.

Corliss J. B., Dymond J., Gordon L. I., Edmond J. M., von Herzen R. P., Ballard R. D., Green K., Williams D., Bainbridge A., Crane K. and van Andel T. H. (1979) Submarine thermal springs on the Galápagos rift. *Science* **203**, 1073–1083.

Craddock P. R., Bach W., Seewald J. S., Rouxel O. J., Reeves E. and Tivey M. K. (2010) Rare earth element abundances in hydrothermal fluids from the Manus Basin, Papua New Guinea: indicators of sub-seafloor hydrothermal processes in back-arc basins. *Geochim. Cosmochim. Acta* **74**, 5494–5513.

Creaser R. A., Sannigrahi P., Chacko T. and Selby D. (2002) Further evaluation of the Re–Os geochronometer in organic-rich sedimentary rocks: a test of hydrocarbon maturation effects in the Exshaw Formation, Western Canada Sedimentary Basin. *Geochim. Cosmochim. Acta* **66**, 3441–3452.

Crusius J., Calvert S., Pederson T. and Sage D. (1996) Rhenium and molybdenum enrichments in sediments as indicators of oxic, suboxic and sulfidic conditions of deposition. *Earth Planet. Sci. Lett.* **145**, 65–78.

Dalai T. K., Singh S. K., Trivedi J. R. and Krishnaswami S. (2002) Dissolved rhenium in the Yamuna River System and the Ganga in the Himalaya: role of black shale weathering on the budgets of Re, Os, and U in rivers and CO_2 in the atmosphere. *Geochim. Cosmochim. Acta* **66**, 29–43.

Davis J. C. (2002) *Statistics and Data Analysis in Geology*, third ed. John Wiley and Sons, New York.

Duyck C., Miekeley N., Porto da Silveira C. L. and Szatmari P. (2002) Trace element determination in crude oil and its fractions by inductively coupled plasma mass spectrometry using ultrasonic nebulization of toluene solutions. *Spectrochim. Acta* **57B**, 1979–1990.

Edmond J. M., Measures C., McDuff R. E., Chan L. H., Collier R., Grant B., Gordon L. I. and Corliss J. B. (1979) Ridge crest hydrothermal activity and the balances of the major and minor elements in the ocean: the Galapagos data. *Earth Planet. Sci. Lett.* **46**, 1–18.

Einsle O., Tezcan F. A., Andrade S. L. A., Schmid B., Yoshida M., Howard J. B. and Rees D. C. (2002) Nitrogenase MoFe-protein at 1.16 Å resolution: a central ligand in the MoFe-cofactor. *Science* **297**, 1696–1700.

Elderfield H. and Schultz A. (1996) Mid-ocean ridge hydrothermal fluxes and the chemical composition of the ocean. *Annu. Rev. Earth Planet. Sci.* **24**, 191–224.

Esser B. K. and Turekian K. K. (1993) The osmium isotopic composition of the continental crust. *Geochim. Cosmochim. Acta* **57**, 3093–3104.

Evans, Jr., H. T. (1978) Molybdenum. In *Handbook of Geochemistry II-4: Vol. II of Handbook of Geochemistry* (eds. K. H. Wedepohl, C. W. Correns, D. M. Shaw, K. K. Turekian and J. Zemann). Springer-Verlag, pp. 42A1–42A3.

Fekete B. M., Vörösmarty C. J. and Grabs W. (2002) High-resolution fields of global runoff combining observed river discharge and simulated water balances. *Global Biogeochem. Cycles* **16**. doi:10.1029/1999GB001254.

Fiege K., Miller C. A., Robinson L. F., Figueroa R. and Peucker-Ehrenbrink B. (2009) Strontium isotopes in Chilean rivers: the flux of unradiogenic continental Sr to seawater. *Chem. Geol.* **268**, 337–343.

Fleischer M. (1959) The geochemistry of rhenium, with special reference to its occurrence in molybdenite. *Econ. Geol.* **54**, 1406–1413.

Fleischer M. (1960) The geochemistry of rhenium – addendum. *Econ. Geol.* **55**, 607–609.

Fleischer M. (1963) New mineral names. *Am. Mineral.* **1948**, 209–217.

Freydier C., Ruiz J., Chesley J., McCandless T. and Munizaga F. (1997) Re–Os isotope systematics of sulfides from felsic igneous rocks: application to base metal porphyry mineralization in Chile. *Geology* **25**, 775–778.

Fukai R. and Meinke W. W. (1962) Activation analyses of vanadium, arsenic, molybdenum, tungsten, rhenium, and gold in marine organisms. *Limnol. Oceanogr.* **7**, 186–200.

Gaillardet J., Viers J. and Dupré B. (2003) Trace elements in river waters. In *Surface and Ground Water, Weathering, and Soils* (ed. J. I. Drever). Treatise on Geochemistry, vol. 5 (eds. H. M. Holland and K. K. Turekian). Elsevier–Pergamon, Oxford.

Graham S. T., Famiglietti J. S. and Maidment D. R. (1999) Five-minute, 1/2°, and 1° data sets of continental watersheds and river networks for use in regional and global hydrologica and climate system modeling studies. *Water Resour. Res.* **35**, 583–587.

Grzymko T. J., Marcantonio F., McKee B. A. and Steward C. M. (2007) Temporal variability of uranium concentrations and $^{234}U/^{238}U$ activity rations in the Mississppi river and its tributaries. *Chem. Geol.* **243**, 344–356.

Hannah J. L., Bekker A., Stein H. J., Markey R. J. and Holland H. D. (2004) Primitive Os and 2316 Ma age for marine shale: implications for Paleoproterozoic glacial events and the rise of atmospheric oxygen. *Earth Planet. Sci. Lett.* **225**, 43–52.

Hauri E. H. and Hart S. R. (1997) Rhenium abundances and systematics in oceanic basalts. *Chem. Geol.* **139**, 185–205.

Hetzel A., Böttcher M. E., Wortmann U. G. and Brumsack H.-J. (2009) Paleo-redox conditions during OAE 2 reflected in Demerara Rise sediment geochemistry (ODP Leg 207). *Palaeogeogr. Palaeoclimatol. Palaeoecol.* **273**, 302–328.

Hirst D. M. (1974) Geochemistry of sediments from 11 Black Sea cores. In *The Black Sea – Geology, Chemistry and Biology: Vol. 20 of Memoir* (eds. E. T. Degens and D. A. Ross). American Association of Petroleum Geologists, Tulsa, Oklahoma, USA, pp. 430–455.

Hodge V. F., Johannesson K. H. and Stetzenbach K. J. (1996) Rhenium, molybdenum, and uranium in groundwater from the southern Great Basin USA: evidence for conservative behavior. *Geochim. Cosmochim. Acta* **60**, 3197–3214.

Huerta-Diaz M. A. and Morse J. W. (1992) Pyritization of trace metals in anoxic marine sediments. *Geochim. Cosmochim. Acta* **56**, 2681–2702.

Huston David L., Sie S. H., Suter G. F., Cooke D. R. and Both R. A. (1995) Trace elements in sulfide minerals from eastern Australian volcanic-hosted massive sulfide deposits: Part I. Proton microprobe analyses of pyrite, chalcopyrite, and sphalerite, and Part II. Selenium levels in pyrite: comparison with $\delta^{34}S$ values and implications for the source of sulfur in volcanogenic hydrothermal systems. *Econ. Geol.* **90**, 1167–1196.

Jaffe L. A., Peucker-Ehrenbrink B. and Petsch S. T. (2002) Mobility of rhenium, platinum group elements and organic carbon during black shale weathering. *Earth Planet. Sci. Lett.* **198**, 339–353.

Jones B. and Manning D. A. C. (1994) Comparison of geochemical indices used for the interpretation of palaeoredox conditions in ancient mudstones. *Chem. Geol.* **111**, 111–129.

Kaback D. S. and Runnels D. D. (1980) Geochemistry of molybdenum in some stream sediments and waters. *Geochim. Cosmochim. Acta* **44**, 447–456.

Kemp D. B., Coe A. L., Cohen A. S. and Schwark L. (2005) Astronomical pacing of methane release in the Early Jurassic period. *Nature* **437**, 396–399.

Kharkar D. P., Turekian K. K. and Bertine K. K. (1968) Stream supply of dissolved silver, molybdenum, antimony, selenium, chromium, cobalt, rubidium and cesium to the oceans. *Geochim. Cosmochim. Acta* **32**, 285–298.

Kim J. and Rees D. C. (1992) Structural models for the metal centers in the nitrogenase molybdenum-iron protein. *Science* **257**, 1677–1682.

Kirk J., Ruiz J., Chesley J., Titley S. and Walshe J. (2001) A detrital model for the origin of gold and sulfides in the Witwatersrand basin based on Re–Os isotopes. *Geochim. Cosmochim. Acta* **65**, 2149–2159.

Kirk J., Ruiz J., Chesley J., Walshe J. and England G. (2002) A major Archean, gold- and crust-forming event in the Kaapvaal Craton, South Africa. *Science* **297**, 1856–1858.

Klinkhammer G. P. and Palmer M. R. (1991) Uranium in the oceans: where it goes and why. *Geochim. Cosmochim. Acta* **55**, 1799–1806.

Koide M., Hodge V., Yang J. S. and Goldberg E. D. (1987) Determination of rhenium in marine waters and sediments by graphite furnace atomic absorption spectrometry. *Anal. Chem.* **59**, 1802–1805.

Koide M., Hodge V. F., Yang J. S., Stallard M., Goldberg E. G., Calhoun J. and Bertine K. K. (1986) Some comparative marine chemistries of rhenium, gold, silver and molybdenum. *Appl. Geochem.* **1**, 705–714.

Korzhinski M. A., Tkachenko S. I., Shmulovich K. I., Taran Y. A. and Steinberg G. S. (1994) Discovery of a pure rhenium mineral at Kudriavy volcano. *Nature* **369**, 51–52.

Large R. R., Danyushevsky L., Hollit C., Maslennikov V., Meffre S., Gilbert S., Bull S., Scott R., Emsbo P., Thomas H., Singh B. and Foster J. (2009) Gold and trace element zonation in pyrite using a laser imaging technique: implications for the timing of gold in orogenic and Carlin-style sediment-hosted deposits. *Econ. Geol.* **104**, 635–668.

Le Riche H. H. (1959) The distribution of certain trace elements in the Lower Lias of southern England. *Geochim. Cosmochim. Acta* **16**, 101–122.

Łetowski F., Serkies J. and Niemiec J. (1966) Application of potential-pH diagrams for determination of the occurrence forms of trace elements in some economic mineral deposits. *Econ. Geol.* **61**, 1272–1279.

Leybourne M. I. and Cameron E. M. (2008) Source, transport, and fate of rhenium, selenium, molybdenum, arsenic, and copper in groundwater associated with porphyry-Cu deposits, Atacama Desert, Chile. *Chem. Geol.* **247**, 208–228.

Ling H.-F., Gao J. F., Zhao K.-D., Jiang S.-Y. and Ma D.-S. (2005) Comment on "Molybdenum isotope evidence for widespread anoxia in Mid-Proterozoic oceans". *Science* **309**, 1017c.

Lipinski M., Warning B. and Brumsack H.-J. (2003) Trace metal signatures of Jurassic/Cretaceous black shales from the Norwegian Shelf and the Barents Sea. *Palaeogeogr. Palaeoclimatol. Palaeoecol.* **190**, 459–475.

Liu G., Chou C.-L., Peng Z. and Yang G. (2008) Abundances and isotopic compositions of rhenium and osmium in pyrite samples from Huaibei coalfield, Anhui, China. *Int. J. Earth Sci.* **97**, 617–621.

Livingstone D. A. (1963) Chemical composition of rivers and lakes. In *Data of Geochemistry*, 6th ed. (ed. M. Fleischer). United States Geological Survey Professional Paper. United States Government, Department of the Interior. G1–G64.

Manheim F. T. (1972) Red Sea geochemistry. *Init. Rep. Deep Sea Drill. Project* **23**, 975–998.

Manheim F. T. and Landergren S. (1978) Molybdenum. In *Handbook of Geochemistry II-4: Vol. II of Handbook of Geochemistry* (eds. K. H. Wedepohl, C. W. Correns, D. M. Shaw, K. K. Turekian and J. Zemann). Springer-Verlag, pp. 42B1–42O2.

Manheim F. T. and Siems D. E. (1972) Chemical analyses of Red Sea sediments. *Init. Rep. Deep Sea Drill. Project* **23**, 923–938.

Mao J., Du A., Seltmann R. and Yu J. (2003) Re–Os ages for the Shamika porphyry Mo deposit and the Lipovy Log rare metal pegmatite, central Urals, Russia. *Miner. Deposita* **38**, 251–257.

Mao J., Wang Y., Lehmann B., Yu J., Du A., Mei Y., Li Y., Zang W., Stein H. J. and Zhou T. (2006) Molybdenite Re–Os and albite $^{40}Ar/^{39}Ar$ dating of Cu–Au–Mo and magnetite porphyry systems in the Yangtze River valley and metallogenic implications. *Ore Geol. Rev.* **29**, 307–324.

Markey R., Stein H. and Morgan J. (1998) Highly precise Re–Os dating for molybdenite using alkaline fusion and NTIMS. *Talanta* **45**, 935–946.

Maslennikov V. V., Maslennikova S. P., Large R. R. and Danyushevsky L. V. (2009) Study of trace element zonation in vent chimneys from the Silurian Yaman-Kasy volcanic-hosted massive sulfide deposit (southern Urals, Russia) using laser ablation-inductively coupled plasma mass spectrometry (LA-ICPMS). *Econ. Geol.* **104**, 1111–1141.

Mason B. and Moore C. B. (1982) *Principles of Geochemistry*. John Wiley and Sons.

Mathur R., Ruiz J. and Munizaga F. (2000) Relationship between copper tonnage of Chilean base-metal porphyry deposits and Os isotope ratios. *Geology* **28**, 555–558.

Mathur R., Ruiz J. and Tornos F. (1999) Age and sources of the ore at Tharsis and Rio Tinto, Iberian Pyrite Belt, from Re–Os isotopes. *Miner. Deposita* **34**, 790–793.

Mathur R., Titley S., Ruiz J., Gibbins S. and Friehauf K. (2005) A Re–Os study of sedimentary rocks and copper–gold ores from Ertsberg District, West Papua, Indonesia. *Ore Geol. Rev.* **26**, 207–226.

McArthur J. M., Donovan D. T., Thirlwall M. F., Fouke B. W. and Mattey D. (2000) Strontium isotope profile of the early Toarcian (Jurassic) oceanic anoxic event, the duration of ammonite biozones, and belemnite palaeotemperatures. *Earth Planet. Sci. Lett.* **179**, 269–285.

McCandless T. E., Ruiz J. and Campbell A. R. (1993) Rhenium behavior in molybdenite in hypogene and near surface environments: implications for Re–Os geochronometry. *Geochim. Cosmochim. Acta* **57**, 889–905.

McLennan S. M. (2001) Relationships between the trace element composition of sedimentary rocks and upper continental crust. *Geochem. Geophys. Geosyst.* **2**. doi:10.1029/2000GC000109.

Meisel T. and Stotter V. (2007) Identifying the sources of PGE, Re and Sb in road dust and soils along highways. *Geochim. Cosmochim. Acta Suppl.* **71**, A650.

Metz S. and Trefry J. H. (2000) Chemical and mineralogical influences on concentrations of trace metals in hydrothermal fluids. *Geochim. Cosmochim. Acta* **64**, 2267–2279.

Meybeck M. (1979) Concentration des eaux fluviales en éléments majeurs et apports en solution aux océans. *Rev. Géol. Dyn. Géogr. Phys.* **21**, 215–246.

Meybeck M. (1988) How to establish and use world budgets of riverine material. In *Physical and Chemical Weathering in Geochemical Cycles* (eds. A. Lerman and M. Meybeck). Kluwer Academic Publishers, pp. 247–272.

Meybeck M. and Helmer R. (1989) The quality of rivers: from pristine stage to global pollution. *Palaeogeogr. Palaeoclimatol. Palaeoecol.* **75**, 283–309.

Meybeck M. and Ragu A. (1995) River discharges to the oceans: an assessment of suspended solids, major ions and nutrients. Technical Report, United Nations Environment Programme.

Miller C. A. (2004) Re–Os dating of algal laminites: reduction enrichment of metals in the sedimentary environment and new geoporphyrins. Master's thesis, University of Saskatchewan, Saskatoon.

Miller C. A. (2009) Surface-cycling of rhenium and its isotopes. Ph.D. thesis, Massachusetts Institute of Technology, Woods Hole Oceanographic Institution.

Millero F. J. and Poisson A. (1981) International one-atmosphere equation of state for seawater. *Deep Sea Res.* **28A**, 625–629.

Mitchell R. H., Laflamme J. H. G. and Cabri L. J. (1989) Rhenium sulphide from the Coldwell complex, northwestern Ontario, Canada. *Mineral. Mag.* **53**, 635–637.

Montgomery R. B. (1958) Water characteristics of Atlantic Ocean and of world ocean.. *Deep Sea Res.* **5**, 134–148.

Morachevskii D. E. and Nechaeva A. A. (1960) Characteristics of migration of rhenium from molybdenites. *Geochemistry* **6**, 648–651.

Morelli R. M., Creaser R. A., Selby D., Kelley K. D., Leach D. L. and King A. R. (2004) Re–Os sulfide geochronology of the Red Dog sediment-hosted Zn–Pb–Ag deposit, Brooks Range, Alaska. *Econ. Geol.* **99**, 1569–1576.

Morelli R. M., Creaser R. A., Selby D., Kontak D. J. and Horne R. J. (2005) Rhenium–osmium geochronology of arsenopyrite in Meguma Group gold deposits, Meguma terrane, Nova Scotia, Canada: evidence for multiple gold-mineralizing events. *Econ. Geol.* **100**, 1229–1242.

Morelli R., Creaser R. A., Seltmann R., Stuart F. M., Selby D. and Graupner T. (2007) Age and source constraints for the giant Muruntau gold deposit, Uzbekistan, from coupled Re–Os–He isotopes in arsenopyrite. *Geology* **35**, 795–798.

Morford J. L. and Emerson S. (1999) The geochemistry of redox sensitive trace metals in sediments. *Geochim. Cosmochim. Acta* **63**, 1735–1750.

Morford J. L., Martin W. R., Kalnejais L. H., François R., Bothner M. and Karle I.-M. (2007) Insights on geochemical cycling of U, Re and Mo from seasonal sampling in Boston Harbor, Massachusetts, USA. *Geochim. Cosmochim. Acta* **71**, 895–917.

Morgan J. W., Golightly D. W. and Dorrzapf Jr., A. F. (1991) Methods for the separation of rhenium, osmium and molybdenum applicable to isotope geochemistry. *Talanta* **38**, 259–265.

Morris A. W. (1975) Dissolved molybdenum and vanadium in the northeast Atlantic Ocean. *Deep Sea Res.* **22**, 49–54.

Morris A. W. and Riley J. P. (1966) The bromide/chlorinity and sulphate/chlorinity ratio in sea water. *Deep Sea Res.* **13**, 699–705.

Morris D. F. C. and Short E. L. (1966) Minerals of rhenium. *Mineral. Mag.* **35**(274), 871–873.

Moyse B. M. (2000) Process, catalyst choices key to producing 30-ppm sulfur fuels. *Oil Gas J.* **98**, 72–74.

Nägler Th. F., Siebert C., Lüschen H. and Böttcher M. E. (2005) Sedimentary Mo isotope record across the Holocene fresh-brackish water transition of the Black Sea. *Chem. Geol.* **219**, 283–295.

Nesheim L., Gautneb H. and Myhr K. (1997) Plant uptake of sulphur and trace elements from pyrite applied on grassland. *Acta Agric. Scand. B: Soil Plant Sci.* **47**, 135–141.

Neubert N., Heri A. R., Voegelin A. R., Nägler T. F., Schlunegger F. and Villa I. M. (2011) The molybdenum isotopic composition in river water: constraints from small catchments. *Earth Planet. Sci. Lett.* **304**, 180–190.

Neubert N., Nägler T. F. and Böttcher M. E. (2008) Sulfidity controls molybdenum isotope fractionation into euxinic sediments: evidence from the modern Black Sea. *Geology* **36**, 775–778.

Noddack I. and Noddack W. (1931) Die Geochemie des Rheniums. *Z. Phys. Chem.* **154A**, 207–244.

Noddack W., Tacke I. and Berg O. (1925) Zwei neue Elemente der Mangangruppe. *Sitzung der physikalisch-mathematischen Klasse* **11**, 400–409.

Patterson J. H., Ramsden A. R., Dale L. S. and Fardy J. J. (1986) Geochemistry and mineralogical residences of trace elements in oil shales from Julia Creek, Queensland, Australia. *Chem. Geol.* **55**, 1–16.

Pearce C. R., Burton K. W. and Pogge von Strandmann P. A. E. (2010) Molybdenum isotope behaviour accompanying weathering and riverine transport in a basaltic terrain. *Earth Planet. Sci. Lett.* **295**, 104–114.

Pearce C. R., Cohen A. S., Coe A. L. and Burton K. W. (2008) Molybdenum isotope evidence for global ocean anoxia coupled with perturbations to the carbon cycle during the Early Jurassic. *Geology* **36**, 231–234.

Petersen R. G., Hamilton J. C. and Myers A. T. (1959) An occurrence of rhenium associated with uraninite in Coconino County, Arizona. *Econ. Geol.* **54**, 254–267.

Peucker-Ehrenbrink B. (2009) Land2Sea database of river drainage basin sizes, annual water discharges, and suspended sediment fluxes. *Geochem. Geophys. Geosyst.* **10**. doi:10.1029/2008GC002356.

Peucker-Ehrenbrink B. and Hannigan R. E. (2000) Effects of black shale weathering on the mobility of rhenium and platinum group elements. *Geology* **28**, 475–478.

Peucker-Ehrenbrink B. and Jahn B.-m. (2001) Rhenium–osmium isotope systematics and platinum group element concentrations: loess and the upper continental crust. *Geochem. Geophys. Geosyst.* **2**. doi:10.1029/2001GC000172.

Peucker-Ehrenbrink B. and Miller M. W. (2007) Quantitative bedrock geology of the continents and large-scale drainage regions. *Geochem. Geophys. Geosyst.* **8**. doi:10.1029/2006GC001544.

Pilipchuk M. F. and Volkov I. I. (1974) Behavior of molybdenum in processes of sediment formation. In *The Black Sea – Geology, Chemistry and Biology: Vol. 20 of Memoir* (eds. E. T. Degens and D. A. Ross). American Association of Petroleum Geologists, Tulsa, Oklahoma, USA, pp. 542–553.

Poplavko E. M., Ivanov V. V., Karasik T. G., Miller A. D., Orekhov V. S., Taliyev S. D., Tarkhov Y. A. and Fadeyeva V. A. (1974) On the concentration of rhenium in petroleum, petroleum bitumens, and oil shales. *Geochem. Int.* **11**, 969–972.

Poulson R. L., Siebert C., McManus J. and Berelson W. M. (2006) Authigenic molybdenum isotope signatures in marine sediments. *Geology* **34**, 617–620.

Power M. R., Pirrie D., Jedwab J. and Stanley C. J. (2004) Platinum-group element mineralization in an As-rich magmatic sulphide system, Talnotry, southwest Scotland. *Mineral. Mag.* **68**, 395–411.

Quinby-Hunt M. S. and Wilde P. (1996) Chemical depositional environments of calcic marine black shales. *Econ. Geol.* **91**, 4–13.

Rahaman W. and Singh S. K. (2010) Rhenium in rivers and estuaries of India: sources, transport and behaviour. *Mar. Chem.* **118**, 1–10.

Raiswell R. and Plant J. (1980) The incorporation of trace elements into pyrite during diagenesis of black shales, Yorkshire, England. *Econ. Geol.* **75**, 684–699.

Ravizza G., Martin C. E., German C. G. and Thompson G. (1996) Os isotopes as tracers in seafloor hydrothermal systems: metalliferous deposits from the TAG hydrothermal area, 26°N Mid-Alantic Ridge. *Earth Planet. Sci. Lett.* **138**, 105–119.

Ravizza G. and Turekian K. K. (1989) Application of the ^{187}Re–^{187}Os system to black shale geochronometry. *Geochim. Cosmochim. Acta* **53**, 3257–3262.

Ravizza G., Turekian K. K. and Hay B. J. (1991) The geochemistry of rhenium and osmium in recent sediments from the Black Sea. *Geochim. Cosmochim. Acta* **55**, 3741–3752.

Rayleigh (1896) Theoretical considerations respecting the separation of gases by diffusion and similar processes. *Philos. Mag.* **42**, 493–498.

Rodhe H. (1992) Modeling biogeochemical cycles. In *Global Biogeochemical Cycles* (eds. S. S. Butcher, R. J. Charlson, G. H. Orians and G. V. Wolfe). Academic Press, pp. 55–72, Ch. 4.

Rosman K. J. R. and Taylor P. D. P. (1998) Isotopic compositions of the elements 1997. *Pure Appl. Chem.* **70**, 217–235.

Roy-Barman M. and Allègre C. J. (1994) $^{187}Os/^{186}Os$ ratios of mid-ocean ridge basalts and abyssal peridotites. *Geochim. Cosmochim. Acta* **58**, 5043–5054.

Rubey W. R. (1951) Geologic history of sea water. *Geol. Soc. Am. Bull.* **62**, 1111–1148.

Scheiderich K., Helz G. R. and Walker R. J. (2010) Century-long record of Mo isotopic composition in sediments of a seasonally anoxic estuary (Chesapeake Bay). *Earth Planet. Sci. Lett.* **289**, 189–197.

Selby D. and Creaser R. A. (2001) Re–Os geochronology and systematics in molybdenite from the Endako porphyry molybdenum deposit, British Columbia, Canada. *Econ. Geol.* **96**, 197–204.

Selby D. and Creaser R. A. (2005) Direct radiometric dating of hydrocarbon deposits using rhenium–osmium isotopes. *Science* **308**, 1293–1295.

Selby D., Creaser R. A. and Fowler M. G. (2007a) Re–Os elemental and isotopic stematics in crude oils. *Geochim. Cosmochim. Acta* **71**, 378–386.

Selby D., Creaser R. A., Stein H. J., Markey R. J. and Hannah J. L. (2007b) Assessment of the ^{187}Re decay constant by cross calibration of Re–Os molybdenite and U–Pb zircon chronometers in magmatic ore systems. *Geochim. Cosmochim. Acta* **71**, 1999–2013.

Seyfried, Jr., W. E. (1987) Experimental and theoretical constraints on hydrothermal alteration processes at mid-ocean ridges. *Annu. Rev. Earth Planet. Sci.* **15**, 317–335.

Seyfried, Jr., W. E. and Mottl M. J. (1982) Hydrothermal alteration of basalt by seawater under seawater-dominated conditions. *Geochim. Cosmochim. Acta* **46**, 985–1002.

Siebert C., Nägler T. F., von Blanckenburg F. and Kramers J. D. (2003) Molybdenum isotope records as a potential new proxy for paleoceanography. *Earth Planet. Sci. Lett.* **211**, 159–171.

Spears D. A., Manzanares-Papayanopoulos L. I. and Booth C. A. (1999) The distribution and origin of trace elements in a UK coal: the importance of pyrite. *Fuel* **78**, 1671–1677.

Stein H. J., Markey R. J., Morgan J. W., Hannah J. L. and Scherstén A. (2001) The remarkable Re–Os geochronometer in molybdenite: how and why it works. *Terra Nova* **13**, 479–486.

Stein H. J., Morgan J. W. and Scherstén A. (2000) Re–Os dating of low-level highly radiogenic (LLHR) sulfides: the Harnäs gold deposit, southwest Sweden, records continental-scale tectonic events. *Econ. Geol.* **95**, 1657–1671.

Stein H. J., Sunblad K., Markey R. J., Morgan J. W. and Motuza G. (1998) Re–Os ages for Archean molybdenite and pyrite, Kuittila-Kivisuo, Finland and Proterozoic molybdenite, Kabeliai, Lithuania: testing the chronometer in a metamorphic and metasomatic setting. *Miner. Deposita* **33**, 329–345.

Student (1908) The probable error of a mean. *Biometrika* **6**, 1–25.

Sugawara K., Okabe S. and Tanka M. (1961) Geochemistry of molybdenum in natural waters (II). *J. Earth Sci. Nagoya Univ.* **9**, 114–128.

Sun W., Bennett V. C., Eggins S. M., Kamenetsky V. S. and Arculus R. J. (2003a) Enhanced mantle-to-crust rhenium transfer in undegassed arc magmas. *Nature* **422**, 294–297.

Sun W., Xie Z., Chen J., Zhang X., Chai Z., Du A., Zhao J., Zhang C. and Zhou T. (2003b) Os–Os dating of copper and molybdenum deposits along the middle and lower reaches of the Yangtze River, China. *Econ. Geol.* **98**, 175–180.

Takahashi Y., Uruga T., Suzuki K., Tanida H., Terada Y. and Hattori K. H. (2007) An atomic level study of rhenium and radiogenic osmium in molybdenite. *Geochim. Cosmochim. Acta* **71**, 5180–5190.

Terada K., Osaki S., Ishihara S. and Kiba T. (1971) Distribution of rhenium in molybdenites from Japan. *Geochem. J.* **4**, 123–141.

Trefry J. H., Butterfield D. B., Metz S., Massoth G. J., Trocine R. P. and Feely R. A. (1994) Trace metals in hydrothermal solutions from Cleft segment on the southern Juan de Fuca Ridge. *J. Geophys. Res.* **99**, 4925–4935.

Tribovillard N., Algeo T. J., Lyons T. and Riboulleau A. (2006) Trace metals as paleoredox and paleoproductivity proxies: an update. *Chem. Geol.* **232**, 12–32.

Tribovillard N., Lyons T. W., Riboulleau A. and Bout-Roumazeilles V. (2008) A possible capture of molybdenum during early diagenesis of dysoxic sediments. *Bull. Soc. Géol. France* **179**, 3–12.

Tuit C. B. (2003) The marine biogeochemistry of molybdenum. Ph.D. thesis, Massachusetts Institute of Technology, Woods Hole Oceanographic Institution.

Turgeon S. and Brumsack H.-J. (2006) Anoxic vs dysoxic events reflected in sediment geochemistry during the Cenomanian–Turonian Boundary Event (Cretaceous) in the Umbria–Marche Basin of central Italy. *Chem. Geol.* **234**, 321–339.

Tuttle M. L. W., Breit G. N., Goldhaber M. B. (2003). Geochemical data from New Albany Shale, Kentucky: a study of metal mobility during weathering of black shales. U.S. Geological Survey Open-File Report 03–207, pp. 1–57.

Tuttle M. L. W., Breit G. N. and Goldhaber M. B. (2009) Weathering of the New Albany Shale, Kentucky: II. Redistribution of minor and trace elements. *Appl. Geochem.* **24**, 1565–1578.

Vine J. D., Tourtelot E. B. and Keith J. R. (1969) Element distribution in some trough and platform types of black shales and associated rocks. U.S. Geological Survey Bulletin 1214-H, H1–H38.

Volborth A., Tarkian M., Stumpfl E. F. and Housley R. M. (1986) A survey of the Pd–Pt mineralization along the 35-km strike of the J-M Reef, Stillwater Complex, Montana. *Can. Mineral.* **24**, 329–346.

Volkov I. I. and Fomina L. S. (1974) Influence of organic material and processes of sulfide formation on distribution of some trace elements in deep-water sediments of Black Sea. In *The Black Sea – Geology, Chemistry and Biology: Vol. 20 of Memoir* (eds. E. T. Degens and D. A. Ross). American Association of Petroleum Geologists, Tulsa, Oklahoma, USA, pp. 456–476.

Walker J. C. G., Hays P. B. and Kasting J. F. (1981) A negative feedback mechanism for the long-term stabilization of Earth's surface temperature. *J. Geophys. Res.* **86**, 9776–9782.

Wedepohl K. H. (1964) Untersuchungen am Kupferschiefer in Nordwestdeutschland; Ein Beitrag zur Deutung der Genese bituminöser Sedimente. *Geochim. Cosmochim. Acta* **28**, 305–364.

Wheat C. G., Mottl M. J. and Rudnicki M. (2002) Trace element and REE composition of a low-temperature ridge-flank hydrothermal spring. *Geochim. Cosmochim. Acta* **66**, 3693–3705.

Whittaker E. J. W. and Muntus R. (1970) Ionic radii for use in geochemistry. *Geochim. Cosmochim. Acta* **34**, 945–956.

Xiong Y. and Wood S. A. (1999) Experimental determination of the solubility of ReO_2 and the dominant oxidation state of rhenium in hydrothermal solutions. *Chem. Geol.* **158**, 245–256.

Xiong Y. and Wood S. A. (2001) Hydrothermal transport and deposition of rhenium under subcritical conditions (up to 200 °C) in light of experimental studies. *Econ. Geol.* **96**, 1429–1444.

Xiong Y. and Wood S. A. (2002) Experimental determination of the hydrothermal solubility of ReS_2 and the Re–ReO_2 buffer assemblage and transport of rhenium under supercritical conditions. *Geochem. Trans.* **3**, 1–10.

Yang J. S. (1991) High rhenium enrichment in brown algae: a biological sink of rhenium in the sea? *Hydrobiologia* **211**, 165–170.

Zhang J., Ren D., Zheng C., Zeng R., Chou C.-L. and Liu J. (2002) Trace element abundances in major minerals of Late Permian coals from southwestern Guizhou province, China. *Int. J. Coal Geol.* **53**, 55–64.

Zhang L., Xiao W., Qin K., Qu W. and Du A. (2005) Re–Os isotopic dating of molybdenite and pyrite in the Baishan Mo–Re deposit, eastern, Tianshan NW China, and its geological significance. *Miner. Deposita* **39**, 960–969.

Zobrist J. and Stumm W. (1981) Chemical dynamics of the Rhine catchment area in Switzerland, extrapolation to the 'pristine' Rhine River input to the ocean. In *River Inputs to Ocean Systems* (eds. J. M. Martin, J. D. Burton and D. Eisma). UNEP/UNESCO/IOC/SCOR, United Nations, New York, pp. 52–63.

Associate editor: Timothy J. Shaw